


RESEARCH PAPER

Ca²⁺ signalling plays a role in celastrol-mediated suppression of synovial fibroblasts of rheumatoid arthritis patients and experimental arthritis in rats

Vincent Kam Wai Wong¹  | Congling Qiu¹ | Su-Wei Xu^{1,6} | Betty Yuen Kwan Law¹ | Wu Zeng¹ | Hui Wang¹ | Francesco Michelangeli² | Ivo Ricardo De Seabra Rodrigues Dias¹ | Yuan Qing Qu¹ | Tsz Wai Chan¹ | Yu Han¹ | Ni Zhang¹ | Simon Wing Fai Mok¹ | Xi Chen¹ | Lu Yu¹ | Hudan Pan¹ | Sami Hamdoun³ | Thomas Efferth³ | Wen Jing Yu¹ | Wei Zhang¹ | Zheng Li¹ | Yuesheng Xie⁴ | Riqiang Luo⁴ | Quan Jiang⁵ | Liang Liu¹

¹State Key Laboratory of Quality Research in Chinese Medicine, Macau University of Science and Technology, Macau, China

²Department of Biological Sciences, University of Chester, Chester, UK

³Department of Pharmaceutical Biology, Institute of Pharmacy and Biochemistry, University of Mainz, Mainz, Germany

⁴Guangdong General Hospital, Guangdong Academy of Medical Sciences, Guangzhou, China

⁵Department of Rheumatology, Guang-An-Men Hospital, China Academy of Chinese Medical Sciences, Beijing, China

⁶Department of Basic Medicine, Zhuhai Health School, Zhuhai, China

Correspondence

Professor Liang Liu, State Key Laboratory of Quality Research in Chinese Medicine, Macau University of Science and Technology, Avenida Wai Long, Taipa, Macau, China.
Email: lliu@must.edu.mo

Funding information

Macao Science and Technology Development Fund, Grant/Award Numbers: 084/2013/A3 and 0022/2018/A1

Background and Purpose: Celastrol exhibits anti-arthritic effects in rheumatoid arthritis (RA), but the role of celastrol-mediated Ca²⁺ mobilization in treatment of RA remains undefined. Here, we describe a regulatory role for celastrol-induced Ca²⁺ signalling in synovial fibroblasts of RA patients and adjuvant-induced arthritis (AIA) in rats.

Experimental Approach: We used computational docking, Ca²⁺ dynamics and functional assays to study the sarcoplasmic/endoplasmic reticulum Ca²⁺ ATPase pump (SERCA). In rheumatoid arthritis synovial fibroblasts (RASFs)/rheumatoid arthritis fibroblast-like synoviocytes (RAFLS), mechanisms of Ca²⁺-mediated autophagy were analysed by histological, immunohistochemical and flow cytometric techniques. Anti-arthritic effects of celastrol, autophagy induction, and growth rate of synovial fibroblasts in AIA rats were monitored by microCT and immunofluorescence staining. mRNA from joint tissues of AIA rats was isolated for transcriptional analysis of inflammatory genes, using siRNA methods to study calmodulin, calpains, and calcineurin.

Key Results: Celastrol inhibited SERCA to induce autophagy-dependent cytotoxicity in RASFs/RAFLS via Ca²⁺/calmodulin-dependent kinase kinase-β-AMP-activated protein kinase-mTOR pathway and repressed arthritis symptoms in AIA rats. BAPTA/AM hampered the in vitro and in vivo effectiveness of celastrol. Inflammatory- and autoimmunity-associated genes down-regulated by celastrol in

Abbreviations: AIA, adjuvant-induced arthritis; AMPK, AMP-activated protein kinase; CaMKK-β, Ca²⁺/calmodulin-dependent kinase kinase-β; ER, endoplasmic reticulum; FLS, fibroblast-like synoviocytes; LC3, light-chain 3; MEFs, mouse embryonic fibroblasts; MTX, methotrexate; RAFLS, rheumatoid arthritis fibroblast-like synoviocytes; RASFs, rheumatoid arthritis synovial fibroblasts; SERCA, sarcoplasmic/endoplasmic reticulum Ca²⁺ ATPase pump

Vincent Kam Wai Wong, Congling Qiu, and Su-Wei Xu contributed equally to this article.

This is an open access article under the terms of the Creative Commons Attribution-NonCommercial License, which permits use, distribution and reproduction in any medium, provided the original work is properly cited and is not used for commercial purposes.

© 2019 The Authors. British Journal of Pharmacology published by John Wiley & Sons Ltd on behalf of British Pharmacological Society.

joint tissues of AIA rat were restored by BAPTA/AM. Knockdown of calmodulin, calpains, and calcineurin in RAFLS confirmed the role of Ca^{2+} in celestrol-regulated gene expression.

Conclusion and Implications: Celestrol triggered Ca^{2+} signalling to induce autophagic cell death in RASFs/RAFLS and ameliorated arthritis in AIA rats mediated by calcium-dependent/-binding proteins facilitating the exploitation of anti-arthritis drugs based on manipulation of Ca^{2+} signalling.

1 | INTRODUCTION

Rheumatoid arthritis (RA) is a systemic autoimmune condition exhibiting polyarthritis and multiple organ disorders (Tsujiura, Saito, Nawata, Nakayamada, & Tanaka, 2008). A variety of cell populations such as lymphocytes, macrophages, and synovial fibroblasts (SLFs) are critically involved in the pathogenesis of RA. Rheumatoid arthritis fibroblast-like synoviocytes (RAFLS) and their primary form, rheumatoid arthritis synovial fibroblasts (RASFs) derived from patient SLFs, are considered key cellular participants in arthritic joints. RASFs in diseased articular tissues over-proliferate and they provide a barrier that hinders the delivery of anti-arthritis agents to the inflamed sites (Bartok & Firestein, 2010). The invasive capacity of RASFs also worsens disease progression by aggravating RA joint erosion via mechanical destruction of normal synovial tissues, neighbouring or distal to the inflamed site (Tolboom et al., 2005). These factors, together with the multidrug- and apoptosis-resistant properties of RASFs (Fang et al., 2013; Igarashi, Hirano, Yahagi, Saika, & Ishihara, 2014; Kim et al., 2011; Maillefert et al., 1996), lead to refractoriness in RA and support RASFs as a promising pharmacological target for the treatment of RA.

Ca^{2+} plays an important role in autoimmunity and inherited immunological dysregulation. In systemic lupus erythematosus, the pro-inflammatory cytokine expression of autoreactive T- and B-lymphocytes upon autoantigens stimulation is manipulated by Ca^{2+} signalling (Tsokos, 2011). During RA progression, autoreactive T-lymphocytes respond to autoantigens through a molecular mechanism similar to that in systemic lupus erythematosus, suggesting the involvement of Ca^{2+} signalling in RA (Sakaguchi et al., 2003). Our recent PCR screen for *in vitro* treatments in RASFs (Dias et al., 2018) suggested a possible link between Ca^{2+} -modulated gene regulation and different pathogenic factors of RA, in which calcium-binding proteins, such as **calmodulin** and **calpains**, are prerequisites for the effective downstream signalling of RA. This cellular Ca^{2+} signalling is closely related to the rigorous maintenance of Ca^{2+} homeostasis, exerted by various Ca^{2+} pumps (Berridge, 2012; Clapham, 2007). The **sarcoplasmic/endoplasmic reticulum (SR/ER) Ca^{2+} -ATPase (SERCA)** is the most extensively studied Ca^{2+} transporter located in the SR/ER membrane (Stammers et al., 2015). Recently, SERCA inhibition has been identified as a novel therapeutic strategy for tumourigenesis by triggering cytotoxicity in cancer cells (Denmeade & Isaacs, 2005; Michelangeli & East, 2011). Suppression of SERCA can severely disrupt Ca^{2+}

What is already known

- Celestrol exhibits anti-arthritis effects by targeting Tregs, Th17 cells, and inhibiting NF- κ B signalling.

What this study adds

- Celestrol inhibits SERCA to induce autophagy-dependent cytotoxicity in RASFs/RAFLS and represses arthritis *in vivo*.
- Block of calcium signalling attenuates the *in vitro* and *in vivo* effectiveness of celestrol.

What is the clinical significance

- Manipulation of Ca^{2+} signalling may represent an alternative approach to the treatment of RA.

homeostasis to induce the ER stress response, thereby causing mitochondrial damage through Ca^{2+} overloading and caspase activation, leading to apoptosis and autophagic cell death (Wong et al., 2013). Moreover, SERCA inhibitors can induce autophagic cell death in both apoptosis- and multidrug-resistant cancer cells (Janssen et al., 2009). For instance, the SERCA inhibitor **thapsigargin** induces autophagy-related cell death in RASFs via ER stress activation (Kato, Ospelt, Gay, Gay, & Klein, 2014). By manipulating Ca^{2+} signalling to induce autophagic cell death, such findings have suggested the potential use of SERCA inhibitors in RASFs that are resistant to apoptosis.

Tripterygium wilfordii Hook F (TwHF), a Chinese medicinal plant, is an effective medication for RA (Tao & Lipsky, 2000; Jiang et al., 2015; Ma, Zhou, Fan, & Sun, 2016). A recent clinical investigation revealed that TwHF-based remedies produced better therapeutic outcomes than disease-modifying antirheumatic drugs alone in controlling symptoms of active RA (Lv et al., 2015). Another randomized trial also demonstrated that TwHF is more effective than the first-line RA drug **sulfasalazine** (Goldbach-Mansky et al., 2009). Additionally, RA patients who failed to respond to conventional therapy were sensitive and showed good tolerance, to multiple therapeutic doses of TwHF (Tao, Younger, Fan, Wang, & Lipsky, 2002). **Celestrol**, a triterpene isolated from TwHF, suppressed autoimmune arthritis and reduce bone damage by modulating osteo-immune crosstalk (Nanjundaiah et al., 2012). Moreover, celestrol inhibited **IL-17A**- and **LPS**-stimulated

migration of RAFLS through the suppression of NF- κ B-mediated MMP-9 expression (Li et al., 2012; Li et al., 2013). Celastrol also suppresses arthritis in adjuvant-induced arthritis (AIA) rats by altering the balance between pathogenic and regulatory T cells in the inflamed joints (Astry et al., 2015). Such beneficial effects have been related to the repression of Th17 cell polarization, associated with the IL-1 β signalling pathway (Cascao et al., 2012; Han et al., 2015). Although celastrol exhibits anti-inflammatory effects by suppressing cell proliferation, invasion, and bone resorption in the treatment of RA (Cascao, Fonseca, & Moita, 2017), mechanistic studies regarding the Ca²⁺-mobilizing effect of celastrol on RA treatment are scarce. Given that celastrol is able to down-regulate a panel of inflammatory- and autoimmunity-associated genes by mobilizing Ca²⁺ in RASFs (Dias et al., 2018), the current study aimed to examine whether celastrol is able to inhibit SERCA and activate Ca²⁺ signalling pathways to mitigate RA, in the well-established experimental AIA model in rats (Astry et al., 2015), which may provide a new strategy for treating RA via activation of Ca²⁺ signalling.

2 | METHODS

2.1 | Cell culture

All cells were obtained from the American Type Culture Collection (Rockville, MD, USA) unless otherwise stated. Immortalized wild-type and Bax-Bak double-knockout mouse embryonic fibroblasts (MEFs) were kindly provided by Professor Shigeomi Shimizu (Tokyo Medical and Dental University, Medical Research Institute, Japan). RASFs were freshly isolated from RA patients in Guangdong General Hospital, Guangdong Academy of Medical Sciences, Guangzhou (China), with research ethics committee approval number: GDREC 2015391H. RAFLS (MH7A) are the immortalized cell line purchased from ATCC. All media were supplemented with 10% FBS and the antibiotics penicillin (50 U·ml⁻¹) and streptomycin (50 μ g·ml⁻¹; Invitrogen, Paisley, Scotland, UK). All cell cultures were incubated at 37°C in a 5% humidified CO₂ incubator.

2.2 | Isolation of RASFs from RA patients

This study involving human tissue samples was approved by the Research Ethics Committee (Guangdong General Hospital, Guangdong Academy of Medical Sciences) with approval number: GDREC 2015391H. RASFs were isolated from synovium from RA patients who had undergone knee surgery for synovectomy. The diagnosis of RA was made according to American Rheumatism Association revised criteria 1987 for classification of RA (Arnett et al., 1988). Synovial strips were cut into pieces and cultured in DMEM containing 20% FBS in 25-cm² culture flask. Medium was changed every 3 days, and the synovial tissues were collected from the cultured medium after 2 weeks. RASFs were trypsinized and diluted with DMEM containing 20% FBS before subculturing into other flasks. Cells were maintained at 37°C in a humidified incubator supplied with 5% of CO₂. The

purification of RASFs was evaluated by staining for CD90. Cultured RASFs from passages 5–7 were employed for experimental studies.

2.3 | Endogenous autophagy detection

In brief, celastrol-treated RASFs or RAFLS cells grown on coverslips were fixed with 4% paraformaldehyde (Sigma) for 20 min and then rinsed with PBS. The cells were then permeabilized in methanol for 2 min and anti-LC3 was used in the analysis. The coverslips were then mounted with FluorSave™ mounting media (Calbiochem, San Diego, CA, USA). Fluorescence localization and quantitation of LC3 autophagosomes were visualized using the API Delta Vision Live-cell Imaging System (Applied Precision Inc., GE Healthcare Company, Washington, USA). The percentage of cells with punctuate immunofluorescence LC3 staining was calculated by the number of immunofluorescence-positive cells (≥ 10 dots per cell) over the total number of cells in the same field. A minimum of 1,000 cells from randomly selected fields were scored.

2.4 | Cytotoxicity assays

Cytotoxicity was assessed using the 3-(4,5-dimethylthiazol-2-yl)-2,5-diphenyltetrazolium bromide (MTT; 5.0 mg·ml⁻¹) assay. Briefly, 4×10^3 Bax-Bak WT or DKO MEFs were seeded per well in 96-well plates. After overnight culture, the cells were then exposed to test compounds (0.039–100 μ mol·L⁻¹) for 72 hr. Cells treated with DMSO were used as control. Subsequently, MTT (10 μ L) was added to each well for 4 hr followed by the addition of 100- μ L solubilization buffer (10% SDS in 0.01 mol·L⁻¹ HCl) and overnight incubation. A₅₇₀ nm was measured on the next day. The percentage of cell viability was calculated by the formula: Cell viability (%) = $A_{\text{treated}}/A_{\text{control}} \times 100$. Data were obtained in triplicate from five independent experiments.

2.5 | Annexin V detection by flow cytometry analysis

Apoptosis was detected by Annexin V staining kit (BD Biosciences, San Jose, CA, USA). In brief, RASFs or RAFLS treated with the indicated doses of celastrol for 24 hr were harvested and detected by flow cytometry using FITC-Annexin V and Propidium Iodide staining, according to the manufacturer's instructions. The population of apoptotic cells were quantitatively determined by flow cytometer (BD FACSAria III, San Jose, CA, USA). Data acquisition and analysis were conducted with CellQuest (BD Biosciences) in triplicate from five independent experiments.

2.6 | Measurement of cytoplasmic calcium dynamics

Intracellular cytosolic Ca²⁺ dynamics was determined using the FLIPR Calcium 6 Assay Kit (Molecular Devices) according to the manufacturer's instructions. In brief, RASFs were plated in black wall/clear bottom 96-multiwell plates (Costar, Tewksbury, MA, USA) at a density

of 10,000 cells per well and incubated overnight before treatment. Next day, the RAFs were treated with calcium 6 reagent for 2 hr at 37°C and 5% CO₂. Indicated concentrations of celastrol or thapsigargin were then added to the wells and immediately subjected to data acquisition on the SpectraMax Paradigm Multi-Mode Microplate Reader (Molecular Devices) at room temperature using a 1-s reading interval throughout five independent experiments.

2.7 | Measurement of intracellular free calcium

Intracellular free calcium level were determined by Fluo-3, AM dye. Briefly, RAFLS cells were washed twice with MEM medium after treatment with indicated concentrations of celastrol for 4 hr. Then, cell suspensions were incubated with 5-μM Fluo-3, AM at 37°C for 30 min. The cells were washed twice with HBSS and then subjected to FACS analysis. At least 10,000 events were analysed. Data were obtained in triplicate from five independent experiments.

2.8 | Computational docking

The co-crystal structure of SERCA complexed with thapsigargin was retrieved from the Protein Data Bank (PDB). To prepare the protein for docking, Autodock Tools-1.5.6rc3 was used to remove crystallographic water molecules and to repair missing atoms. The output files after preparation was in PDBQT format. The ligands to be docked were drawn using ChemDraw software and converted into 3D structures using Open Babel. All 3D structures were saved in PDBQT format. The docking grid box was created and defined by the thapsigargin binding site on SERCA. Celastrol was docked on the selected sites of SERCA using Autodock 4. At each grid point, the energy of a particular ligand configuration was predicted. Docking parameters were set to 250 runs and 2,500,000 energy evaluations for each cycle using the Lamarckian Algorithm. The binding energies and the number of conformations in each cluster were attained from the docking log files (dlg).

2.9 | Measurement of SERCA activity

Ca²⁺ ATPase (SERCA1A) was extracted and purified from hind leg muscle of female rabbits. The effect of celastrol on Ca²⁺ ATPase activity was then determined using the enzyme-coupled method utilizing LDH and pyruvate kinase as previously described (Michelangeli, Colyer, East, & Lee, 1990). The SERCA inhibitory raw data were fitted to the allosteric concentration-effect equation using Figure P (Biosoft, Cambridge, UK):

$$\text{Activity} = \text{minimum activity} + (\text{maximum activity} - \text{minimum activity}) / (1 + ([I]/IC_{50})^P).$$

Data were obtained in triplicate from five independent experiments.

2.10 | Protein extraction and western blotting

The antibody-based procedures used in this study comply with the recommendations made by the *British Journal of Pharmacology*. After drug treatment, adherent and floating cells were lysed with RIPA. Protein concentrations were determined using the Bio-Rad protein assay (Bio-Rad Laboratories, Inc., Hercules, CA, USA). After electrophoretic separation, gels were blotted and stained with primary antibodies. The binding of the antibody was visualized by peroxidase-coupled secondary antibody using the ECL Western Blotting Detection Reagents (Invitrogen, Paisley, Scotland, UK). Band intensities were quantified by using the software ImageJ (NIH, Bethesda, MD, USA). Data were obtained from five independent experiments.

2.11 | LC-MS/MS measurement of ATP metabolites

Celastrol-treated RAFLS were harvested in 12 ml of ice-cold PBS. The cell pellet was then treated with 150 μl of 15% trichloroacetic acid (TCA) containing 7.5 μl of 20.0-μM [¹³C, ¹⁵N]ATP as internal standard and placed on ice for 10 min. After centrifugation at 12,100 × g for 15 min, the acidic supernatant was separated and neutralized twice with 80 μl mixture of triethylamine and 1,1,2-trichlorotrifluoroethane (a volume ratio of 45 to 55), the samples were then ready for LC-MS/MS analysis. A Thermo Fisher TSQ LC-MS/MS system consisted of an Accela Autosampler, an Accela pump, and a Quantum Access triple quadrupole mass spectrometer. Data acquisition was performed with the Xcalibur software version 2.0.7, and data processing was carried out using the Thermo LCquan 2.5.6 data analysis program. The chromatographic separation was performed using XTerra-MS C18 column (150 mm × 2.1 mm i.d., 3.5 μm, Waters, Milford, MA). The two eluents were as follows: (A) 5-mM HA-0.5% DEA in water, pH 10 was adjusted with acetic acid; and (B) 50% acetonitrile in water. The mobile phase consisted of linear gradients of A and B: 0–15 min, 100–80% A (v/v); 15–35 min, 80–70% A; 35–45 min, 70–45% A; 45–46 min, 45–0% A; 46–50 min, 0–0% A; and 51–70 min, 100–100% A. The liquid flow rate was set at 0.3 ml·min⁻¹, and the column temperature was maintained at 35°C. Data were obtained from five independent experiments.

2.12 | Dual luciferase assay

Briefly, RAFLS were co-transfected with *Renilla* and one of the luciferase reporter plasmid of ATF6, CHOP, GRP-78, and GRP94 respectively. The next day, cells were treated with indicated concentrations of celastrol and thapsigargin for 24 hr. Cells then harvested with 100 μl of passive lysis buffer before luminescence measurements. According to the protocol of the dual luciferase reporter assay system (Promega Corp., E1910), 100 μl of the firefly luciferase reagent (LARII) was first added to each test sample, followed by addition of 100 μl of the *Renilla* luciferase reagent and firefly quenching (Stop & Glo). The data were represented as the ratio of firefly to *Renilla* luciferase activity (Fluc/RLuc) from five independent experiments.

2.13 | AIA in rats and treatment

All animal care and experimental procedures were approved by the Animal Ethical Committee of Department of Health and Supervision, Macao Special Administrative Region of China, and carried out in accordance to the "Institutional Animal Care and User Committee guidelines" of the Macau University of Science and Technology. Animal studies are reported in compliance with the ARRIVE guidelines (Kilkenny, Browne, Cuthill, Emerson, & Altman, 2010; McGrath & Lilley, 2015) and with the recommendations made by the *British Journal of Pharmacology*. Drug preparation, treatment, and animal data collection were conducted blindly and independently by three investigators.

The AIA model was established using 6-week-old male Sprague Dawley rats (RRID:MGI:5651135) weighing 130 ± 20 g (four per cage) which were purchased from Guangdong Medical Lab Animal Center. The animals were housed in a temperature-controlled room with 12-hr light/dark cycles and given ad libitum access to food and water.

Arthritis was induced in rats by inoculation with complete Freund's adjuvant. Non-viable desiccated *Mycobacterium tuberculosis* (BD, USA) was emulsified in mineral oil (Sigma, USA) to yield $5 \text{ mg}\cdot\text{ml}^{-1}$ of *M. tuberculosis*. The rats were injected intradermally at the base of the tail with $100\text{-}\mu\text{l}$ of this emulsion. The first signs of inflammation were observed on Day 9 after adjuvant injection. Arthritic scores were evaluated and recorded every 3 days. Each paw was evaluated and scored individually on a scale from 0 to 4. The scoring criteria was as follows: 0, no evidence of erythema and swelling; 1, erythema and mild swelling confined to the tarsals or ankle joint; 2, erythema and mild swelling extending from the ankle to the tarsals; 3, erythema and moderate swelling extending from the ankle to metatarsal joints; and 4, erythema and severe swelling encompass the ankle, foot and digits, or ankylosis of the limb.

Forty-eight male rats were randomly divided into five experimental groups as follows: (a) healthy control group ($n = 8$) without treatments; (b) vehicle-treated control group ($n = 8$), AIA rats receiving the same vehicle and administration route of the drug in each experiment; (c) positive control group ($n = 8$), AIA rats receiving (by gavage) MTX ($7.6 \text{ mg}\cdot\text{kg}^{-1}\cdot\text{week}^{-1}$ in a volume of $10 \text{ ml}\cdot\text{kg}^{-1}$ body weight). (d) AIA rats receiving $1 \text{ mg}\cdot\text{kg}^{-1}$ of celestrol (Cel; $n = 8$); (e) AIA rats receiving $1 \text{ mg}\cdot\text{kg}^{-1}$ of celestrol + $3.5 \text{ mg}\cdot\text{kg}^{-1}$ BAPTA/AM (BM; $n = 8$). AIA rats were treated i.p. with celestrol daily in the first 19 days and then treated every 2 days until Day 36, whereas BM was administered daily. Celestrol (China cdmust, A0106) and BAPTA/AM (Santa Cruz, USA) were dissolved in the vehicle (PEG400: H₂O: Ethanol = 6:3:1) and administered i.p. in a volume of $1 \text{ ml}\cdot\text{kg}^{-1}$ body weight. MTX was dissolved in a vehicle of propylene glycol: Tween-80: normal saline, 50:5:45.

At the end of the treatment period, the rats were killed (cervical dislocation during pentobarbital anaesthesia) and the left hind paw was amputated and fixed in 4% PFA, then scanned using in vivo microCT scanner (SkyScan 1176, Bruker, Belgium). The following scanning parameters were used to obtain high-quality images of the joint:

$35\text{-}\mu\text{m}$ resolution, 85 kV, $385 \mu\text{A}$, 65-ms exposure time, 0.7° rotation step in 360° , and a 1-mm Al filter. The images were reconstructed using NRecon software (Bruker-micro CT, Belgium).

MicroCT score was obtained from five disease-related indices of the microCT analysis for calcaneus (bone mineral density, bone volume fraction, cortical mineral density, trabecular number, and total porosity). MicroCT score was calculated using the formula as follows: (Acquired value - minimum value)/(maximum value - minimum value) or $1 - (\text{Acquired value} - \text{minimum value})/(\text{maximum value} - \text{minimum value})$. The final microCT score is equally averaged from these five indices of disease.

2.14 | Immunofluorescent staining of rat synovial tissues

Synovial tissues from all treatment groups were fixed and embedded in paraffin for microtome sectioning and immunofluorescence staining. After deparaffinization, the tissue sections ($5\mu\text{m}$ thick) were subjected to antigen retrieval (EnVision™ FLEX Target Retrieval Solution, High pH (50×)). Anti-LC3B or anti-vimentin were used in the analysis. The coverslips were then mounted with FluorSave™ mounting media (Calbiochem, San Diego, CA, USA) for fluorescence imaging. The expression of LC3 and vimentin was captured by API DeltaVision Live-cell Imaging System (Applied Precision Inc., GE Healthcare Co., Washington, USA).

2.15 | siRNA transfection, RNA extraction, and cDNA synthesis

RASFs were transfected with a mixture of siRNAs using Lipofectamine® 3000 (Invitrogen) according to the manufacturer's protocol. To maximize the knockdown efficiency for the calcium binding protein (calmodulin, calpains, and calcineurin), the siRNA of these gene isoforms were mixed together before the transfection: siRNA CALM1 + CALM2 + CALM3 for calmodulin, siRNA CAPN1 + CAPN2 for calpains, and siRNA PPP3CA + PPP3CB + PPP3CC for calcineurin. All siRNA were purchased from Qiagen (Cambridge, USA).

RNA was extracted from the (AIA) animal joint tissues or immortalized RASFs using FavorPrep™ Blood/Cultured Cell Total RNA Purification Mini Kit (Favorgen Biotech Corp.). RNA concentration was determined using the NanoDrop 2000c Spectrophotometer (Thermo Scientific) and $1 \mu\text{g}$ of total RNA was used to synthesize the corresponding cDNA using the Transcriptor Universal cDNA Master mix (Roche, USA).

2.16 | Real-time quantitative PCR

Quantitative PCR was performed using cDNA prepared from $1 \mu\text{g}$ of RNA of treated immortalized RASFs, with PowerUp™ SYBR® Green Master Mix (Applied Biosystems) in the ViiA™ 7 Real Time PCR System (Applied Biosystems), together with primers synthesized (Tech Dragon Ltd., Hong Kong) using our own designed templates. Primer

sequences were designed employing ThermoFisher Scientific's online OligoPerfect™ Designer software and then verified with NCBI's Primer-BLAST software to confirm specific recognition of the target genes. Gene expression levels were normalized to GAPDH, (control), and analysed using the $2^{-\Delta\Delta CT}$ method. Five independent experiments with six replicates per group were analysed for each primer. Primer sequences are designed as below:

ADGRE5	Forward 5'-CTTCCCGATTCTTCGACAA-3' Reverse 5'-TTCCATCAGTTCATCCACCA-3'	FGF10	Forward 5'-GCATGTGCGGAGCTACAATC-3' Reverse 5'-GCTGACCTTCCCGTCTTCT-3'
BMP1	Forward 5'-CAACACGTTCCGGCAGTTATG-3' Reverse 5'-CACTGGTGGATGTCACCTTG-3'	GLMN	Forward 5'-GGGCACACAGACCAGCTATT-3' Reverse 5'-AAGGCATCGAACAAACAGGAC-3'
CALM1	Forward 5'-TCAGCTGACCGAAGAACAGA-3' Reverse 5'-GACCCAGTGACCTCATGACA-3'	HRH1	Forward 5'-ACCCCAAGGAGATGAAATC-3' Reverse 5'-GCCTGCATGTGCACAATATC-3'
CALM2	Forward 5'-ATGCTGATGGTAATGGCACA-3' Reverse 5'-CAAACACACGGAATGCTTCT-3'	IFNAR1	Forward 5'-AAGCTCAGATTGGTCCTCCA-3' Reverse 5'-CCATCCAAAGCCCACATAAC-3'
CALM3	Forward 5'-ATGGGAATGGCTACATCAGC-3' Reverse 5'-TCAGCCTCCCTGATCATCTC-3'	IK	Forward 5'-CAAAGGACCTGGGTCTACCA-3' Reverse 5'-TTCTGGCTTCTTCAGCGATT-3'
CAPN1	Forward 5'-TCAGAGTGGAAACAACGTGGA-3' Reverse 5'-GAACTCCCGCATGAAGTCTC-3'	IL1R1	Forward 5'-ATTGATGTTTCGTCCTGTCC-3' Reverse 5'-TGAATCCTGGAGGCTTGTTCC-3'
CAPN2	Forward 5'-AGGCATACGCCAAGATCAAC-3' Reverse 5'-AGGGGGCTTCTTCAACTCAT-3'	IL4R	Forward 5'-CCGCCTCGTGGCTATAATAA-3' Reverse 5'-CAGGGCAAGAGCTTGGAAG-3'
CAST	Forward 5'-GAAGTCGATGAGGCCAAAAGC-3' Reverse 5'-CATCTTTATCCGTGGCTGGT-3'	LEPR	Forward 5'-AATGCATTTTCCAGCCAATC-3' Reverse 5'-TGGCTTACCACAGAATCAG-3'
CD40	Forward 5'-GAGATCAATTTTCCCGACGA-3' Reverse 5'-CGACTCTCTTGCCATCCTC-3'	NFATC3	Forward 5'-TGTTATGCTGGGTCCCTTTC-3' Reverse 5'-CAGAAGCATTGAGCCACGTA-3'
CMTM1	Forward 5'-ATCACCCAAGCCAATGAGTC-3' Reverse 5'-GCAAGTGGTGAAGGGTTAGC-3'	NFKB1	Forward 5'-GCCTCTAGATATGGCCACCA-3' Reverse 5'-TCAGCCAGCTGTTTCATGTC-3'
ERBB2	Forward 5'-AACCAGCTGGCTCTCACACT-3' Reverse 5'-CAGAACTCTCTCCCGCAGCAG-3'	NFRKB	Forward 5'-TCGAGCTGTTCTTCCAGTT-3' Reverse 5'-GGAAGAGGGCAGCTAATTCC-3'
		NFX1	Forward 5'-CCAAGTTTATGGCCTGGAGA-3' Reverse 5'-TTTCAAGCACACCTGTCAGC-3'
		PPP3CA	Forward 5'-GGGTGCATCAATTCTTCGAC-3' Reverse 5'-CCCGACTCAAAGAGCTTCA-3'

PPP3CB	Forward 5'-ATGGGATACCCAGGGTTGAT-3' Reverse 5'-TGGTTTTCTCTCCGAAGG-3'
PPP3CC	Forward 5'-TTGGACCTGTGTGACCTG-3' Reverse 5'-AATAAGAGCACCTCGGACA-3'
STAT3	Forward 5'-GGCCATCTTGAGCACTAAGC-3' Reverse 5'-CTGGGTCTTACCGCTGATGT-3'
TLR6	Forward 5'-ACTGACCTTCTGGATGTGG-3' Reverse 5'-CTGGCAGCTCTGGAAGAAAT-3'
TOLLIP	Forward 5'-CTGAAAGCCATCCAGGACAT-3' Reverse 5'-ATCTGCAGCAGGGAGTTGAT-3'
TRAP1	Forward 5'-CTTGAAAACTGCGTCACA-3' Reverse 5'-GATGGTGATGGTGCCTTTCT-3'
GAPDH	Forward 5'-CAGCCTCAAGATCATCAGCA-3' Reverse 5'-TGTGGTCATGAGTCTTCCA-3'

2.17 | Data and statistical analysis

The data and statistical analysis comply with the recommendations of the *British Journal of Pharmacology* on experimental design and analysis in pharmacology (Curtis et al., 2018). Data are expressed as means \pm SEM. All the histological samples were scored blindly and independently by two investigators. Each experiment was conducted independently at least five times. Statistical analysis was carried out with GraphPad Prism 7 (RRID:SCR_002798). Data were analysed with Student's two-tailed *t* test or one-way ANOVA. Dunnett's or Tukey's post hoc test was carried out only if $P \leq .05$ was accepted. Values of $P < .05$ were taken to indicate statistically significant differences between means.

2.18 | Materials

All chemicals and reagents were purchased from Sigma, unless otherwise stated. The following reagents from other suppliers were used: thapsigargin (Calbiochem, 586005, USA), **compound C** (Calbiochem, 171260, USA), BAPTA/AM (Santa Cruz, USA), bafilomycin A1 (Calbiochem, 196000, USA), **STO-609** (Calbiochem, 570250, USA), celastrol (cdmust, A0106, China), **methotrexate** (MTX; LC labs, MA,

USA), RIPA (CST, 9806, USA), Fluo-3, AM (Life Technologies, F14218, USA), EnVision™ FLEX Target Retrieval Solution, High pH (50 \times ; DAKO, DM828, USA), antibodies light-chain 3B (LC3B) rabbit mAb (Cell signaling, 2775/3868, USA, RRID:AB_915950), phospho-p70S6 kinase (Thr³⁸⁹) rabbit mAb (CST, 9205, USA), p70S6 kinase rabbit mAb (CST, 9202, USA), phospho-AMP-activated protein kinase (AMPK; Thr¹⁷²) rabbit mAb (CST, 2531, USA), AMPK rabbit mAb (CST, 2532, USA), vimentin mouse mAb (Abcam, 8978, USA), anti- β -of actin mouse monoclonal IgG1 (Santa Cruz, sc-47778, USA), rabbit anti-mouse IgG (H + L) secondary antibody TRITC (Invitrogen, PA1-28565, USA), and GOXMO TRITC HIGH XADS (Invitrogen, A16083, USA).

2.19 | Nomenclature of targets and ligands

Key protein targets and ligands in this article are hyperlinked to corresponding entries in <http://www.guidetopharmacology.org>, the common portal for data from the IUPHAR/BPS Guide to PHARMACOLOGY (Harding et al., 2018), and are permanently archived in the S186 of Concise Guide to PHARMACOLOGY 2017/18 (Alexander, Christopoulos et al., 2017; Alexander, Fabbro et al., 2017a,b; Alexander, Kelly et al., 2017; Alexander, Striessnig et al., 2017).

3 | RESULTS

3.1 | Celastrol targets SERCA for Ca²⁺ mobilization in RASFs/RAFLS

Flow cytometry analysis of fluo-3 AM dye-stained RAFLS showed that celastrol released Ca²⁺ in a time- and concentration-dependent manner (Figure 1a). Celastrol is a triterpenoid compound and another triterpenoid, saikosaponin-d, caused the accumulation of cytosolic Ca²⁺ via inhibition of SERCA (Wong et al., 2013). Thus celastrol may also target SERCA for Ca²⁺ release and we therefore studied the changes in calcium dynamics, induced by celastrol in the presence of a known SERCA inhibitor, **thapsigargin**. As shown in Figure 1b, FLIPR calcium 6 assay demonstrated that either thapsigargin or celastrol alone changed the calcium dynamics in RASFs, but celastrol was much less potent than thapsigargin. Pre-incubation of RASFs with thapsigargin abolished the effects of celastrol on Ca²⁺ mobilization (Figure 1b), suggesting that celastrol targeted the SERCA-dependent Ca²⁺ stores which had been depleted by thapsigargin treatment. As a negative control, pretreatment with a different kinase inhibitor, compound C, which inhibits AMPK, with no reported interaction with SERCA, did not affect the changes in calcium dynamics induced by celastrol.

Computational docking results further revealed that celastrol and thapsigargin preferentially bound to the same pharmacophore on SERCA. The lowest binding energies for thapsigargin and celastrol were -12.37 and -10.27 kcal \cdot mol⁻¹ respectively (Figure 1c). Using purified sarcoplasmic reticulum (SR) membranes from rabbit skeletal muscle, that expressed the SERCA1A isoform (Wong et al., 2013),

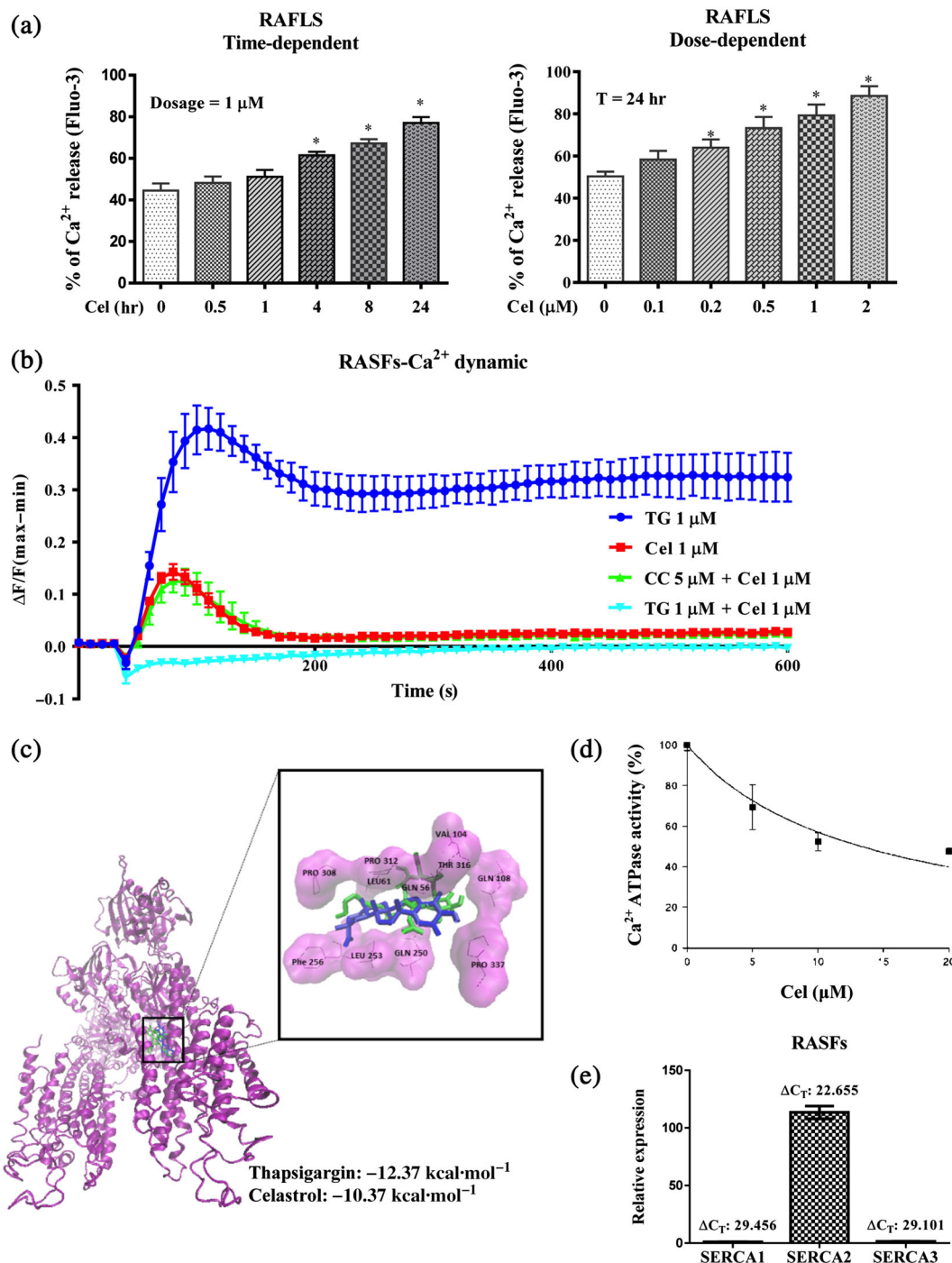


FIGURE 1 Effect of celastrol on SERCA Ca²⁺ pump activity. (a) Time- and concentration-dependent flow-cytometric analysis of celastrol-mediated Ca²⁺ mobilization in RAFLS using Fluo-3 AM dye. The data shown are the means \pm SEM from five independent experiments.

* $P < .05$, significantly different from untreated group. (b) Ca²⁺ dynamics change of thapsigargin in celastrol-treated RASFs. RASFs stained with the FLIPR Calcium 6 Assay Kit were treated with 1- μM thapsigargin (TG; positive control), 1- μM celastrol (Cel), and 1- μM celastrol with or without pretreatment with compound C (CC; 5 μM) or thapsigargin (1 μM) for 2 hr, and then immediately subjected to measurements of Ca²⁺ dynamics using the FLIPR Tetra High-Throughput Cellular Screening System. The data shown in the chart are the means \pm SEM from five independent experiments. (c) Computational docking of the SERCA pump with celastrol. (d) Effect of celastrol in Ca²⁺-ATPase (SERCA) activity in the SR of skeletal muscles. (e) Expression of SERCA isoforms in RASFs. ΔC_T values of three of the SERCA isoforms are indicated on the bar chart. The data shown are the means \pm SEM from five independent experiments.

celastrol inhibited SERCA1A in a concentration-dependent manner (Figure 1d), and the data fit to an allosteric concentration-effect equation. RT-PCR analysis further identified the SERCA 2 isoform as the

most abundant type of SERCA in RASFs (Figure 1e), suggesting that celastrol was also effective in the inhibition of the SERCA2 isoform for calcium mobilization, as indicated in Figure 1b.

3.2 | Celastrol induces autophagic flux to activate autophagic cell death in RASFs and RAFLS

Mobilization of cytosolic Ca^{2+} induces autophagy and autophagic cell death in cancer cells (Wong et al., 2013). We therefore tested the effects of celastrol on autophagy and cell death in RASFs/RAFLS and found that autophagy and cell death in RASFs/RAFLS was induced by celastrol, in a concentration- and time-dependent manner (Figures 2a and S1A and B). The celastrol-induced endogenous autophagic LC3-II puncta formation in RAFLS (Figure 2b) and LC3-II protein conversion in RASFs (Figure 2c) were similarly blocked by the **PI3K** inhibitor, **wortmannin**, which is an autophagy inhibitor (Klionsky et al., 2016). Of note, celastrol significantly increased the rate of LC3-II conversion in the presence of the lysosomal protease inhibitor bafilomycin A1, compared with the administration of the inhibitors alone (Figure 2d). These results are therefore consistent with the premise that celastrol-increased Ca^{2+} mobilization induces autophagy and the resultant cell death of SLFs through the enhancement of autophagic flux.

3.3 | Celastrol activates CaMKK β -AMPK-mTOR signalling pathway to induce Ca^{2+} -dependent autophagy in RASFs/RAFLS

We have previously shown that autophagy can be activated by calcium mobilization via the **Ca^{2+} /calmodulin-dependent kinase kinase- β (CaMKK β)-AMPK-mTOR** pathway (Wong et al., 2013). Here, we showed that celastrol activated AMPK phosphorylation and reduced the phosphorylated form of p70S6K, a downstream target of **mTOR** (Figure 3a). In addition, the AMPK inhibitor compound C (non-toxic dose: 5 μM) significantly inhibited celastrol-induced endogenous LC3-II puncta formation and LC3-II protein conversion in both RAFLS and RASFs (Figure 3b,c). As autophagy can be activated by an upstream kinase of AMPK, the CaMKK β (Wong et al., 2013), treatment with the CaMKK β inhibitor, STO-609 (non-toxic dose: 25 μM), abolished celastrol-induced endogenous LC3-II puncta formation and LC3-II protein conversion in RAFLS and RASFs (Figure 3d,e), suggesting that celastrol increased the level of cytosolic Ca^{2+} which induced autophagy induction through the CaMKK β -AMPK-mTOR pathway.

3.4 | Calcium chelator BAPTA/AM abolishes celastrol-induced autophagic cell death in RASFs/RAFLS and apoptosis-resistant fibroblasts

The synovial environment in RA patients favours the survival of FLS and prevents their removal by apoptosis and this resistance of FLS to apoptosis has been considered as a major therapeutic challenge (Kim et al., 2011). Thus, induction of autophagic cell death might serve as an alternative way of eliminating apoptosis-resistant RASFs/RAFLS in RA (Bartok & Firestein, 2010; Turner & Filer, 2015). Hence, we further validated whether block of Ca^{2+} release affects celastrol-induced autophagic cell death in RASFs/RAFLS. Of note, the calcium chelator BAPTA/AM suppressed celastrol-induced endogenous autophagic

LC3-II puncta formation in RAFLS (Figure 4a) and inhibited LC3-II protein conversion in RASFs (Figure 4b). Concomitantly, annexin V-PI staining showed that both BAPTA/AM and the autophagy inhibitor, wortmannin, reduced celastrol-mediated autophagic cell death (Figure 4c). These findings suggest that mobilization of Ca^{2+} is necessary for celastrol to induce autophagy and autophagic cell death in SLFs. Furthermore, we mimicked the apoptosis-resistant phenotype of RAFLS using apoptosis-resistant fibroblasts, for example, Bax-Bak double-knockout (DKO) MEFs. Interestingly, while the resistant factor of DKO fibroblasts was 1.77 to >14 times more resistant to cell death by the anti-inflammatory agents, **leflunomide**, **tacrolimus**, **baricitinib**, sulfasalazine, and **hydroxychloroquine**, **colchicine**, celastrol, and MTX showed little difference in cell death sensitivity in both Bax-Bak wild-type and DKO fibroblasts (Figure 5a). As expected, celastrol was able to induce autophagic puncta formation and autophagic cell death in these apoptosis-resistant fibroblasts, whereas co-administration of BAPTA/AM substantially blocked the celastrol-induced autophagic effects and cell death (Figure 5b,c). All these findings supported the view that celastrol eliminated SLFs and apoptosis-resistant fibroblasts through calcium-induced autophagic cell death.

3.5 | Celastrol-mediated Ca^{2+} release induces energy loss and ER stress activation in RAFLS

Abnormal cytosolic Ca^{2+} levels can disrupt calcium homeostasis and activate the ER stress response in cells, which further induces the release and overload of Ca^{2+} in mitochondria, leading to cytochrome *c* release and mitochondrial membrane potential loss (Denmeade & Isaacs, 2005). By LC-MS/MS analysis, we found that the amounts of **ATP**, **ADP**, and **AMP** metabolites in the mitochondria was decreased in the celastrol-treated RAFLS (Figure 5d), suggesting mitochondrial damage in RAFLS which can be caused by the perturbation of calcium homeostasis (Todd, Lee, & Glimcher, 2008). As disruption of calcium homeostasis can also lead to activation of the ER stress response as well as apoptosis and autophagic cell death (Todd, Lee, & Glimcher, 2008), we therefore investigated whether celastrol could activate the ER stress response using the dual-luciferase reporter assays. Both celastrol and thapsigargin, a positive regulator for the elevation of cytosolic Ca^{2+} , markedly increased the expression of ER stress markers ATF6, CHOP, GRP78, and GRP94 in RAFLS (Figure 5e), indicating that celastrol may similarly induce apoptosis and autophagic cell death via Ca^{2+} release and ER stress activation in RAFLS.

3.6 | Celastrol suppresses AIA in rats via mobilization of Ca^{2+}

Although celastrol has exhibited anti-arthritis effect in vivo (Li et al., 2013; Venkatesha, Yu, Rajaiah, Tong, & Moudgil, 2011) through inhibition of cytokines, chemokines, and inflammatory mediators (Cascao, Fonseca, & Moita, 2017), the role of celastrol-mediated Ca^{2+} in RA therapy remains unclear. Therefore, the possible anti-arthritis effect

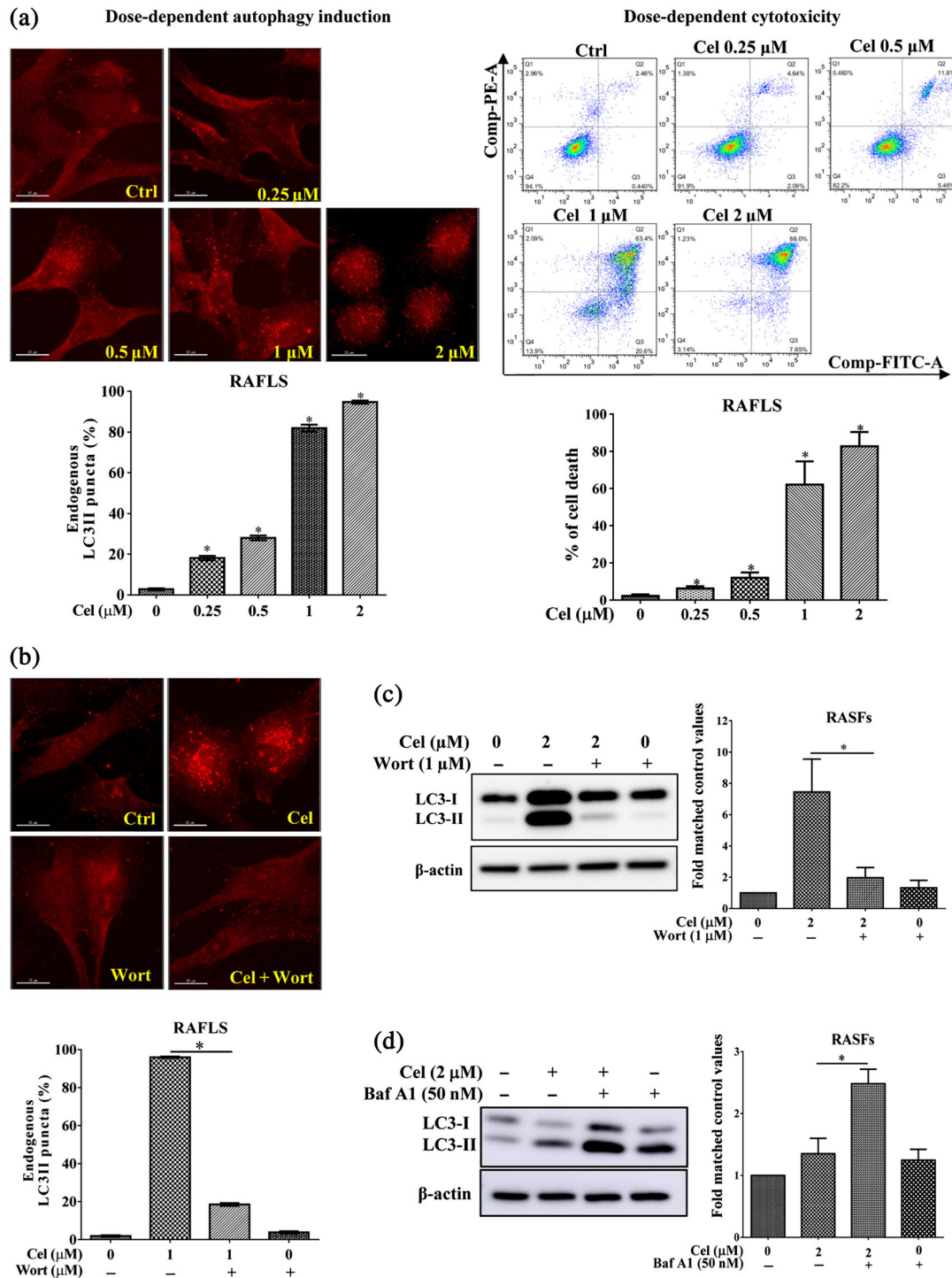


FIGURE 2 Effect of celastrol-induced autophagy in RA synovial fibroblasts. (a) The correlation between celastrol-mediated autophagy and cytotoxicity. The concentration-dependent cytotoxicity of celastrol (Cel) was measured by annexin V-propidium iodide flow cytometry in parallel with dose-dependent autophagic puncta formation in RAFLS treated with DMSO or 0- to 2- μ M celastrol for 24 hr. Y-axis: PI; X-axis: annexin-V FITC. (b) Effect of wortmannin (Wort) in celastrol-induced autophagy in RAFLS. RAFLS were treated with DMSO or 2- μ M celastrol for 24 hr in the presence or absence of 1- μ M wortmannin. The cells were counted only with the increased puncta pattern of LC3 fluorescence (≥ 10 dots/cell) in immunofluorescence-positive cells over the total number of cells in the same field. Fluorescence images were captured at 60 \times magnification; scale bar, 15 μ m. Bar charts demonstrate the quantitation of the increase in autophagic cells. (c) Effect of Wort in celastrol-mediated LC3-II conversion. RASFs were treated with DMSO or 2- μ M celastrol for 24 hr in the presence or absence of 1- μ M wortmannin. (d) Effect of celastrol in autophagic flux. RASFs were treated with DMSO or 2- μ M celastrol in the presence or absence of lysosomal protease inhibitors, Bafilomycin A1 (BafA1) 50 nM for the indicated times. Western blotting with antibodies against LC3 conversion (LC3-I, 18 kDa; LC3-II, 16 kDa) and β -actin. The data are expressed as fold matched control values relative to the DMSO-treated control. The data shown are the mean \pm SEM of five independent experiments. * $P < .05$, significantly different from DMSO-treated control or celastrol-treated group

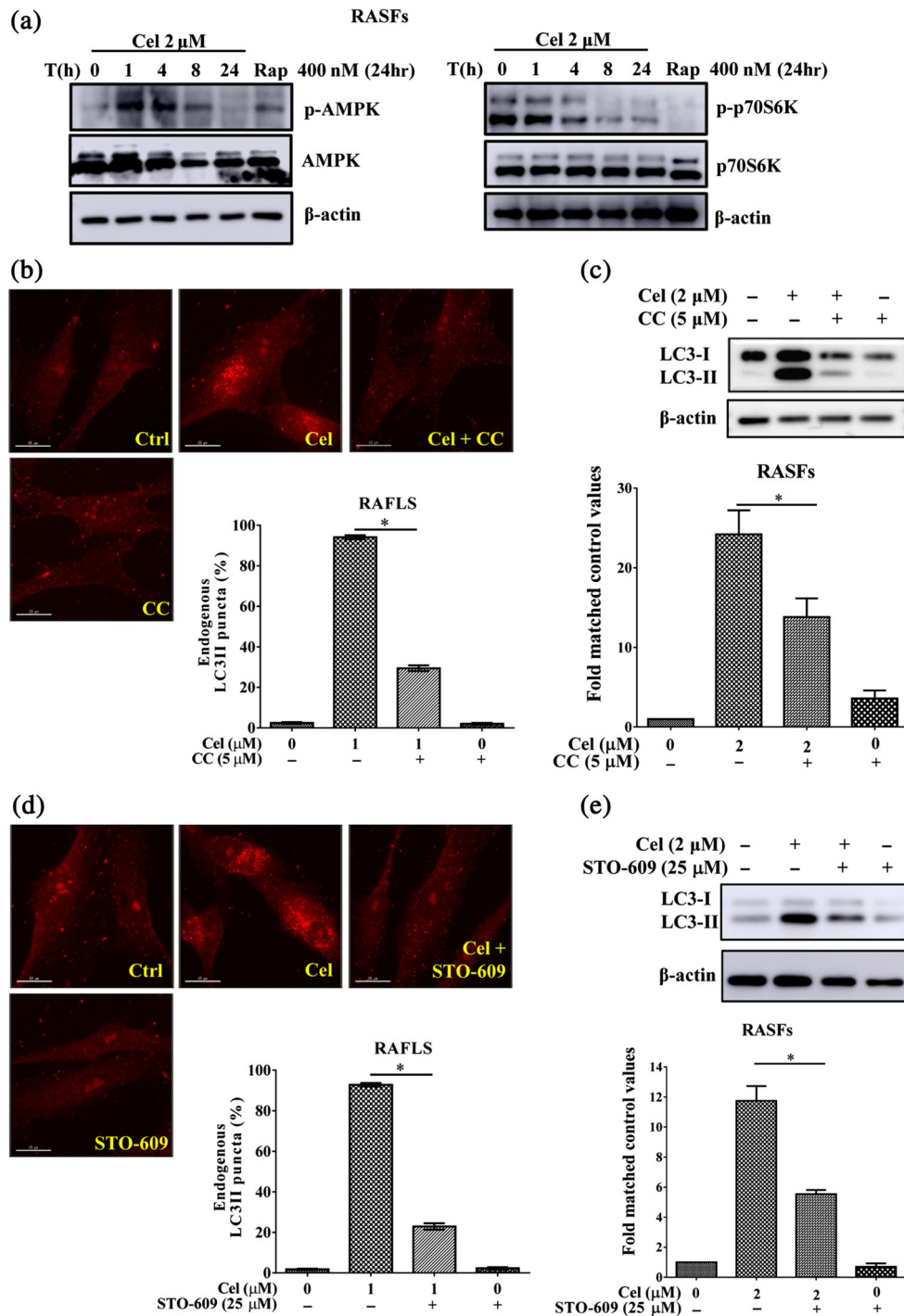


FIGURE 3 Effect of celastrol in CaMKK β -AMPK-mTOR signalling cascade. (a) Activation of the AMPK-mTOR signalling pathways by celastrol (Cel). RASFs were treated with DMSO or 2- μ M celastrol for the indicated times, and rapamycin (Rap, 400 nM) was used as a positive control. Western blot analysis with antibodies against p-AMPK, total AMPK, p-p70S6K, total p70S6K, and β -actin. (b) Effect of compound C (CC) on celastrol-induced autophagic puncta formation in RAFLS. RAFLS were treated with DMSO or 1- μ M celastrol for 24 hr with or without 5- μ M compound C before fluorescence microscopic analysis. Bar chart represents the quantitation of autophagic cells with an increased percentage of LC3 puncta. (c) Effect of compound C in celastrol-mediated LC3-II conversion. RASFs were treated with DMSO or 2- μ M celastrol for 24 hr in the presence or absence of 5- μ M compound C. (d) Effect of CaMKK β inhibitor in celastrol-induced autophagy in RAFLS. RAFLS were treated with DMSO or 1- μ M celastrol for 24 hr with or without 25- μ M STO-609 (CaMKK β inhibitor) before fluorescence microscopy scoring. Bar chart represents the quantitation of autophagic cells with increased percentage of LC3 puncta. (e) Effect of CaMKK β inhibitor, STO-609 in celastrol-mediated LC3-II conversion. RASFs were treated with DMSO or 2- μ M celastrol for 24 hr in the presence or absence of 25- μ M STO-609. Western blotting with antibodies against LC3 conversion (LC3-I, 18 kDa; LC3-II, 16 kDa) and β -actin. The data are expressed as fold matched control values relative to the DMSO-treated control. The data are expressed as the mean values \pm SEM of five independent experiments. * $P < .05$, significantly different from DMSO-treated control group

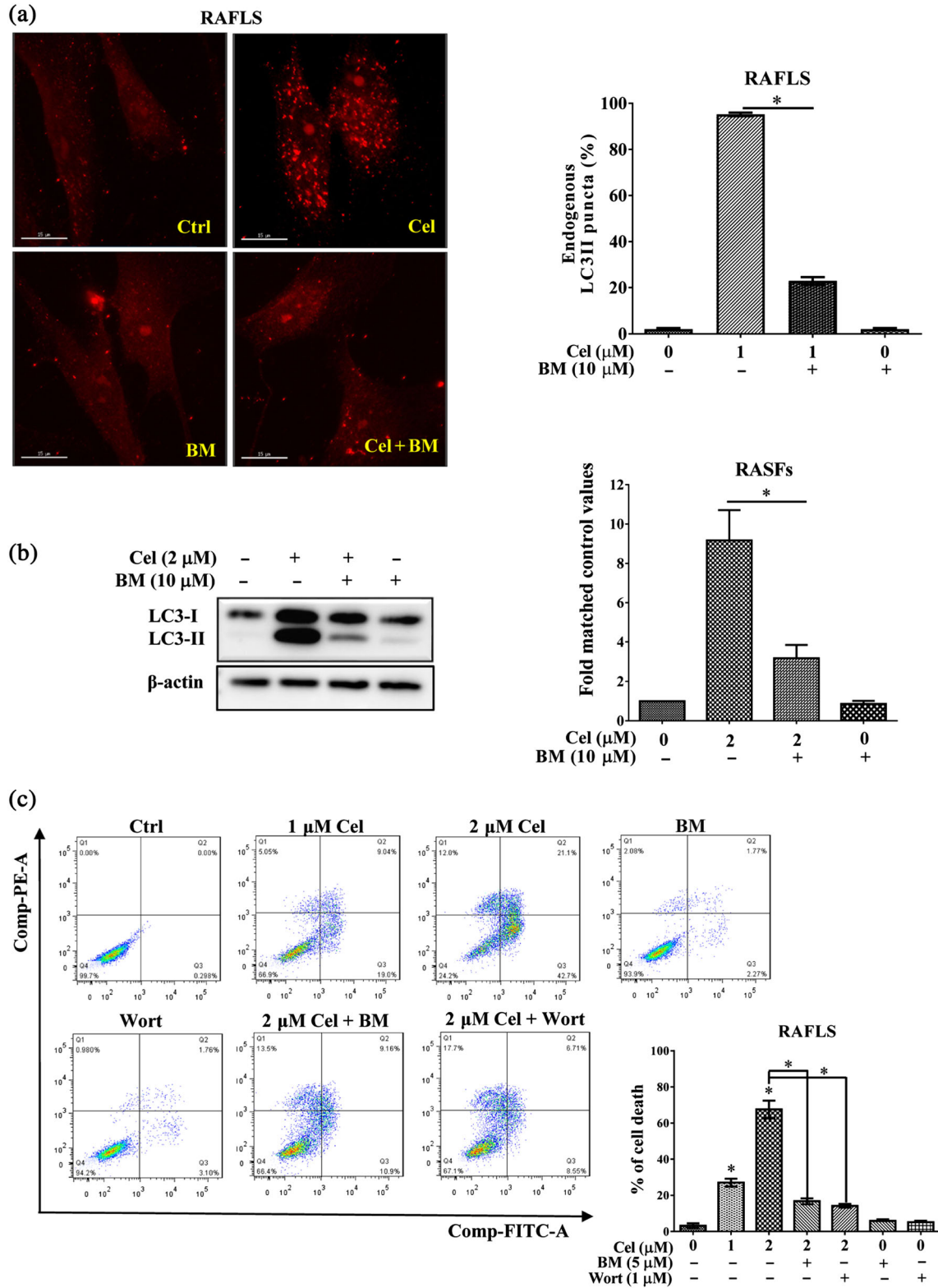


FIGURE 4 Effect of Ca^{2+} chelator BAPTA/AM in celastrol-mediated autophagy and cell death in RAFLS. (a) Autophagic effect of celastrol (Cel) in RAFLS in the presence of Ca^{2+} chelator BAPTA/AM. RAFLS were treated with DMSO or 1- μ M celastrol for 24 hr in the presence or absence of 10- μ M BAPTA/AM (BM). Bar charts representing the quantitation of cells with increased autophagic puncta are shown. Fluorescence images were captured at 60 \times magnification; scale bar, 15 μ m. (b) Effect of BAPTA/AM in celastrol-mediated LC3-II conversion in RASFs. Western blotting with antibodies against LC3 conversion (LC3-I, 18 kDa; LC3-II, 16 kDa) and β -actin. Bar chart represents the quantitation of LC3-II conversion. (c) Recovery effect of BAPTA/AM and Wort in celastrol-mediated autophagic cell death in RAFLS. RAFLS treated with celastrol for 24 hr were measured using flow cytometry after annexin V-PI staining. Y-axis: PI; X-axis: annexin-V FITC. The data are expressed as the mean values \pm SEM of five independent experiments. * $P < .05$, significantly different from DMSO-treated control or celastrol-treated group

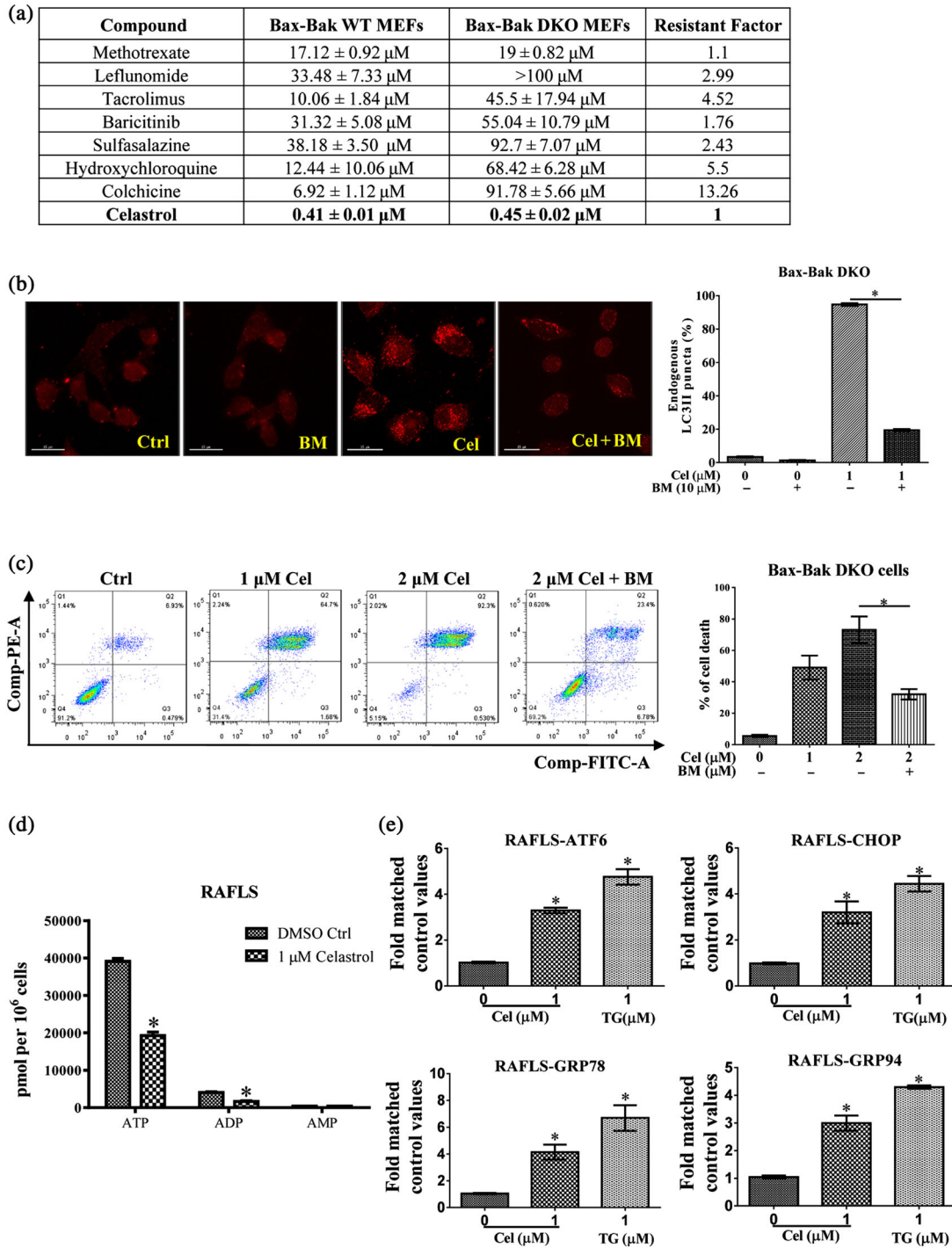


FIGURE 5 Activation of ER stress and Ca^{2+} signalling in celastrol-mediated autophagic cell death in the apoptosis-resistant fibroblasts. (a) Comparison of drug-resistance effects on various anti-inflammatory agents caused by celastrol in apoptosis-defective Bax-Bak DKO fibroblasts. MEFs were incubated with compounds for 72 hr, and the MTT cytotoxicity assay was performed to determine their cytotoxicity. The IC_{50} values shown on the chart are the means \pm SEM from five independent experiments. (b) Effect of BAPTA/AM (BM) in celastrol (Cel)-induced autophagy in Bax-Bak DKO apoptosis-defective fibroblasts. Bar charts show the quantitation of the increase in autophagic cells. Fluorescence images were captured at 60 \times magnification; scale bar, 15 μm . (c) Effect of BAPTA/AM in celastrol-induced autophagic cell death in the apoptosis-defective fibroblasts. The percentage of cell death in celastrol-treated Bax-Bak DKO MEFs with or without BAPTA/AM was measured using flow cytometry after annexin V staining. (d) Effect of celastrol in mitochondrial ATP generation in RAFLS. RAFLS treated with DMSO or 1- μM celastrol for 24 hr were subjected to mitochondrial extraction. Mitochondrial ATP, ADP, and AMP were measured by HPLC-MS ($N = 6$). (e) Activation of the ATF6, CHOP, GRP78, and GRP94 signalling in celastrol-treated RAFLS. ATF6-, CHOP-, GRP78-, and GRP94-containing dual-luciferase reporter plasmid-transfected RAFLS were treated with DMSO or 1- μM celastrol for 24 hr, and thapsigargin (TG, 1 μM) was used as a positive control. Cell lysates were harvested for dual-luciferase reporter assay. The data are expressed as the mean values \pm SEM of five independent experiments. * $P < .05$, significantly different from DMSO-treated control or celastrol-treated group

of celastrol via Ca^{2+} mobilization was examined in the AIA rat model. As shown in Figure 6a,b, celastrol significantly reduced the arthritic score and hind paw volume without affecting other organs or body weight in comparison with vehicle-treated AIA rats (Figure S2). Interestingly, addition of the calcium chelator BAPTA/AM partly decreased the anti-arthritic effect of celastrol (Figure 6c). MicroCT analysis was used to evaluate the severe swollen joints and bone destruction in the vehicle-treated AIA rats by direct comparisons of bone mineral density, bone volume fraction, cortical mineral density, trabecular number, and total porosity to other treatment groups. As shown in Figures 6d and S2C and D, the overall microCT and radiological scores indicated that inflammation and bone destruction were significantly better with the treatment of celastrol or MTX. MicroCT analysis of bone volume fraction, trabecular number, and total porosity indicated that the AIA rats treated with the combination of celastrol and BAPTA/AM displayed severe bone destruction compared to the rats treated with celastrol alone. As shown in Figures 6c–d, S2B–D, and Video S1, the mean microCT score dropped significantly from 0.54 to 0.33, while the mean radiological score rose from 1.33 to 1.83. The induction of autophagy in the synovial joints of the rat model after celastrol treatment was then examined by fluorescent immunohistochemical analysis. The antibodies LC3B (red) was used to detect the formation of autophagosomes, while vimentin (green) was used as a marker to indicate the proliferation and epithelial–mesenchymal transition of fibroblasts which are critical to the pathogenesis of RA. As shown in Figure 6e, the administration of celastrol ($1 \text{ mg}\cdot\text{kg}^{-1}$) alone clearly triggered the induction of autophagy when compared with untreated and healthy controls. In addition, the expression of vimentin was significantly suppressed in celastrol-treated rats compared with AIA rats. The suppression of vimentin was greater after celastrol than that in AIA rats treated with $7.6 \text{ mg}\cdot\text{kg}^{-1}$ of MTX, suggesting that the therapeutic efficacy of celastrol had been achieved at $1 \text{ mg}\cdot\text{kg}^{-1}$. The celastrol-induced effects on autophagy activation and vimentin suppression were mitigated by co-treatment of celastrol and BAPTA/AM, which decreases intracellular Ca^{2+} levels. Accordingly, the anti-arthritic effect of celastrol was partly attributable to the elevated Ca^{2+} and its downstream activation of the autophagic pathway.

3.7 | The calcium-dependent/-binding proteins calmodulin, calpains, and calcineurin play critical roles in celastrol-mediated anti-arthritis effect in AIA rats

Celastrol mobilized cytosolic Ca^{2+} in patient-derived RASFs and regulated 23 out of 370 genes associated with inflammation and autoimmunity (Dias et al., 2018). Accordingly, expression of these Ca^{2+} -induced genes was validated using the joint tissues from our AIA model. Real-time PCR analysis indicated that except for **CD40**, **GLMN**, and **TRAP1**, the expression of the other 20 genes was almost significantly down-regulated in our AIA model treated with celastrol, whereas co-treatment with the Ca^{2+} chelator, BAPTA/AM abolished the down-regulation of genes mediated by celastrol (Figure 7). These results suggest the possible therapeutic role of Ca^{2+} signalling in RA condition.

Ca^{2+} is a second messenger that is required for the signal transduction of many cellular processes (Clapham, 2007), and calmodulin, calcineurin, and calpains are well-known downstream modulators of Ca^{2+} -dependent enzymes, such as protein kinases, phosphatases, and proteases (Villalobo A, 2018). Therefore, the role of celastrol-mediated Ca^{2+} signalling in the regulation of inflammatory and autoimmunity-associated gene expression was verified by knockdown of these three Ca^{2+} -binding/-dependent proteins. To ensure high efficiency in transfection and knockdown of genes, we used the RAFLS cells for validation of these 23 genes of interest by specific siRNA knockdown of calmodulin, calcineurin, and calpains individually, prior to celastrol treatment. In Figure S3, effective knockdown of the target genes was achieved by transfecting the cocktail of siRNAs specific to different gene isoforms of calmodulin (**CALM1** + **CALM2** + **CALM3**), calpains (**CAPN1** + **CAPN2**), and calcineurin (**PPP3CA** + **PPP3CB** + **PPP3CC**). Under the same gene knockdown condition, 21 out of 23 genes (fold change values <0.75) were down-regulated compared to RAFLS transfected with scrambled control siRNA followed by celastrol (Ctrl siRNA + Cel), while one gene, **CD40**, was up-regulated (fold change value >1.5) when compared to cells transfected with control siRNA (Ctrl siRNA alone; Figure 8). Importantly, the individual knockdown of calmodulin, calcineurin, or calpains restored the gene expression pattern of celastrol-treated RAFLS to different extents (Genes siRNA + Cel). These findings suggest that the three Ca^{2+} -dependent regulators, calmodulin, calcineurin, and calpains, are the upstream regulators of these 22 inflammatory genes in response to treatment with celastrol.

As shown in the proposed mechanisms depicted in Figure 9, 22 out of 23 genes were modulated entirely or partly, by at least two of the investigated Ca^{2+} -dependent/-binding proteins, and calcineurin was the most frequently involved protein. For example, the expression of **CD40**, **HRH1**, **LEPR**, **NFRKB**, **STAT3**, **TOLLIP**, and **TRAP1** was modulated by calmodulin and calcineurin; **IFNAR1** and **TLR6** were modulated by calpains and calcineurin; the remaining genes, including **BMP1**, **CAST**, **ERBB2**, **FGF10**, **GLMN**, **IK**, **NFATC3**, **NFKB1**, and **NFX1**, were suppressed by all three Ca^{2+} -dependent/-binding proteins. Furthermore, four genes were modulated by only one of the Ca^{2+} -dependent/-binding proteins: **CMTM1** was suppressed only by calmodulin, **ADGRE5** and **IL4R** were suppressed only by calpains, and **IL1R1** was suppressed only by calcineurin. These data suggest that several calmodulin- and calpain-independent pathways are activated in the transcription of selected inflammatory and autoimmunity-associated genes after treatment with celastrol.

4 | DISCUSSION

Celastrol, the major bioactive component of the Chinese medical plant *Tripterygium wilfordii* Hook F, has been used as a conventional treatment for RA in China and other Asian countries, demonstrating significant anti-arthritic effects in both experimental arthritis models and RA patients (Tao & Lipsky, 2000; Tao, Younger, Fan, Wang, & Lipsky, 2002; Goldbach-Mansky et al., 2009; Venkatesha, Yu, Rajaiah, Tong,

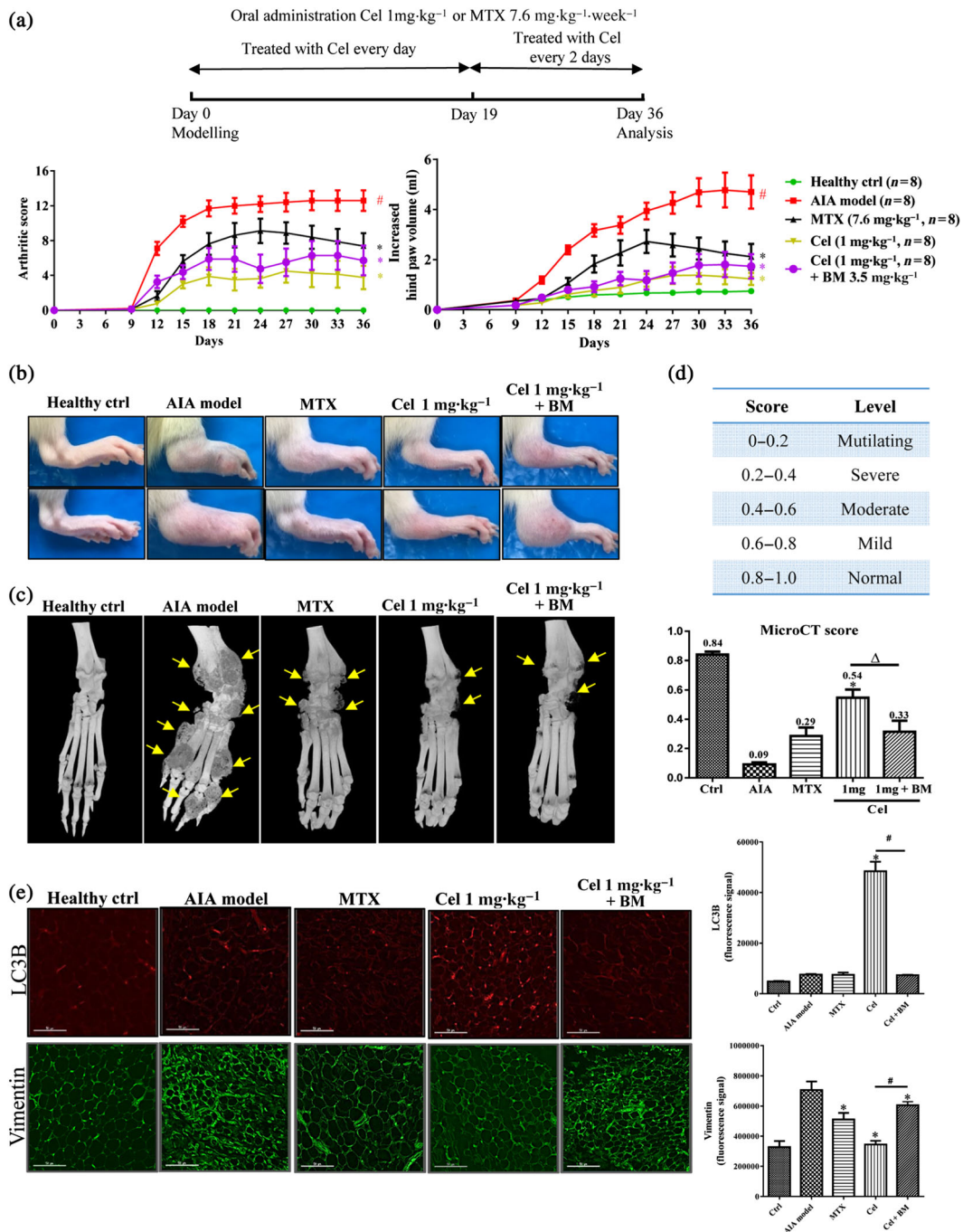


FIGURE 6 The anti-arthritic effect of celastrol on adjuvant-induced arthritis (AIA) in rats via calcium mobilization. (a) The arthritic scores and hind paw swelling of celastrol (Cel)-treated AIA rats. (b) Representative images of hind paw swelling from AIA rats after treatment. (c) Representative microCT images of hind joints of AIA rats after treatment. Yellow arrows indicate bone erosion. Healthy control group and four groups of rats were treated with vehicle, MTX (7.6 mg·kg⁻¹), celastrol (1 mg·kg⁻¹), or celastrol (1 mg·kg⁻¹) combined with BAPTA/AM (BM; 3.5 mg·kg⁻¹) after arthritis induction for 36 days. Hind paw volumes (ml) and arthritic scores were determined every 3 days. The data are expressed as the mean values ± SEM (n = 8). (d) The microCT scores of celastrol-treated AIA rats. MicroCT scores were obtained from five disease-related indexes of microCT analyses of the calcaneus - bone mineral density, bone volume fraction, cortical mineral density, trabecular number, and total porosity. The data are expressed as the mean values ± SEM from n = 8 rats per group. *P < .05, significantly different from vehicle-treated AIA group. #P < .05, significantly different from healthy control group. ΔP < .05 for microCT score comparison between celastrol treatment group and celastrol plus BAPTA/AM treatment group. (e) The autophagic effect and proliferative rate of synovial fibroblasts in synovium of AIA rat treated by celastrol. Synovium tissues isolated from five rats of each treatment group were section and immune-stained with antibodies against autophagic marker LC3B and synovial fibroblasts marker vimentin prior to secondary antibody (GOXMO TRITC HIGH XADS) treatment. The fluorescence images shown are the representative images from five independent animals. Bar charts show the ImageJ (RRID:SCR_003070) quantitation of the fluorescence signal from LC3B and vimentin. *P < .05, significantly different from vehicle-treated AIA group. #P < .05, significantly different from Cel + BM-treated AIA group

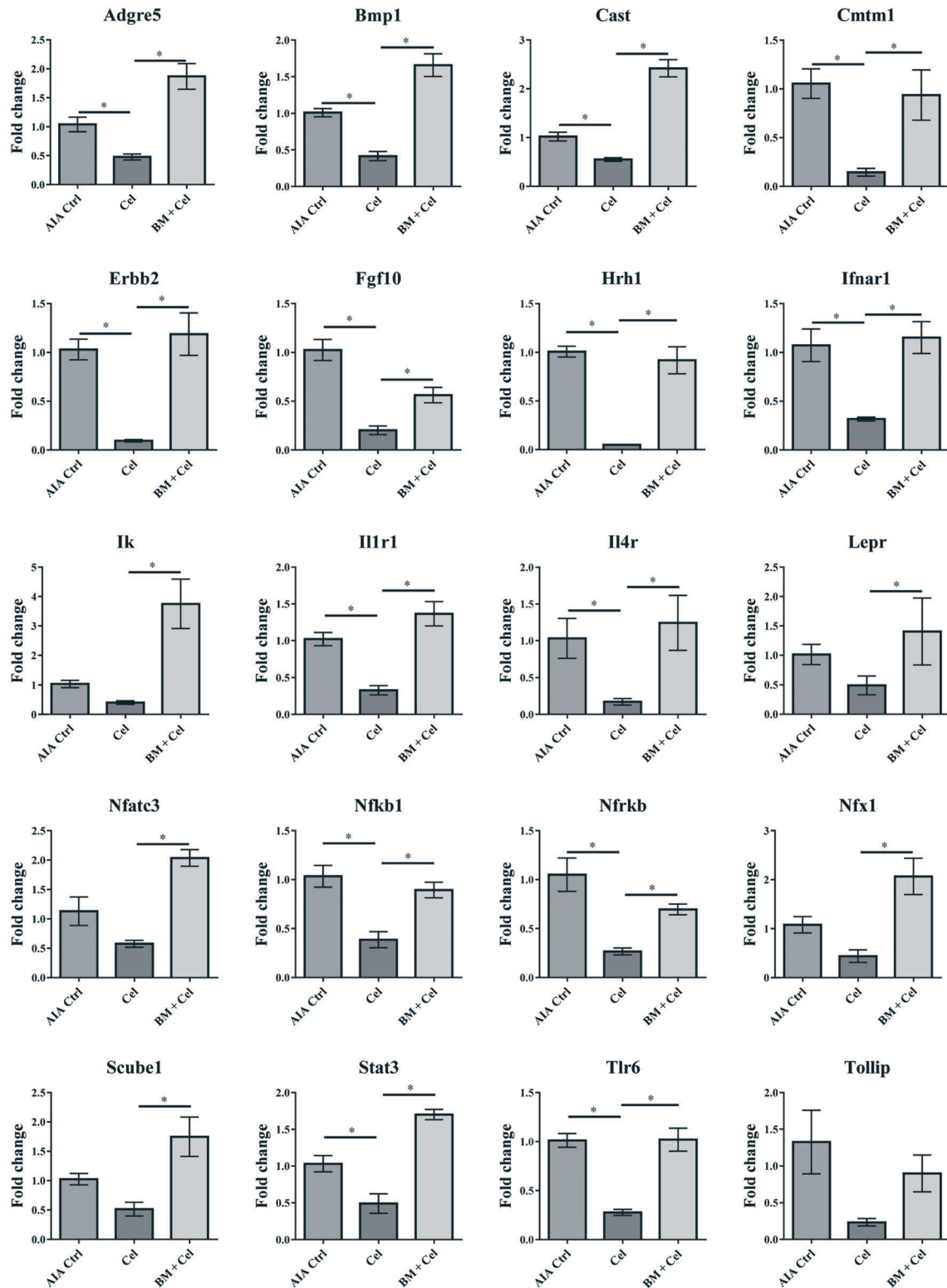


FIGURE 7 Effect of BAPTA/AM in the expression of celastrol-regulated inflammatory and autoimmunity genes in the joint tissues of AIA rats. After the completion of drug treatment in the AIA rat model, the joint tissues harvested from the AIA vehicle control group (AIA Ctrl), celastrol 1 mg·kg⁻¹ group (Cel), and celastrol 1 mg·kg⁻¹ plus BAPTA/AM group (BM + Cel) were prepared for RNA isolation, reverse transcription into cDNA, and real-time qPCR analysis of 23 genes of interest related to inflammation and autoimmunity (Dias et al., 2018). Among these 23 genes identified in the human RASF studies, 20 of their counterparts in rats have been identified as being down-regulated by celastrol-induced increase of calcium concentration in a similar pattern. After RT-qPCR, gene expression was normalized to GAPDH, relative to AIA vehicle control, and analysed using the $2^{-\Delta\Delta CT}$ method. The data are presented as the mean \pm SEM, **P* < .05, significantly different from AIA or Cel + BM-treated group

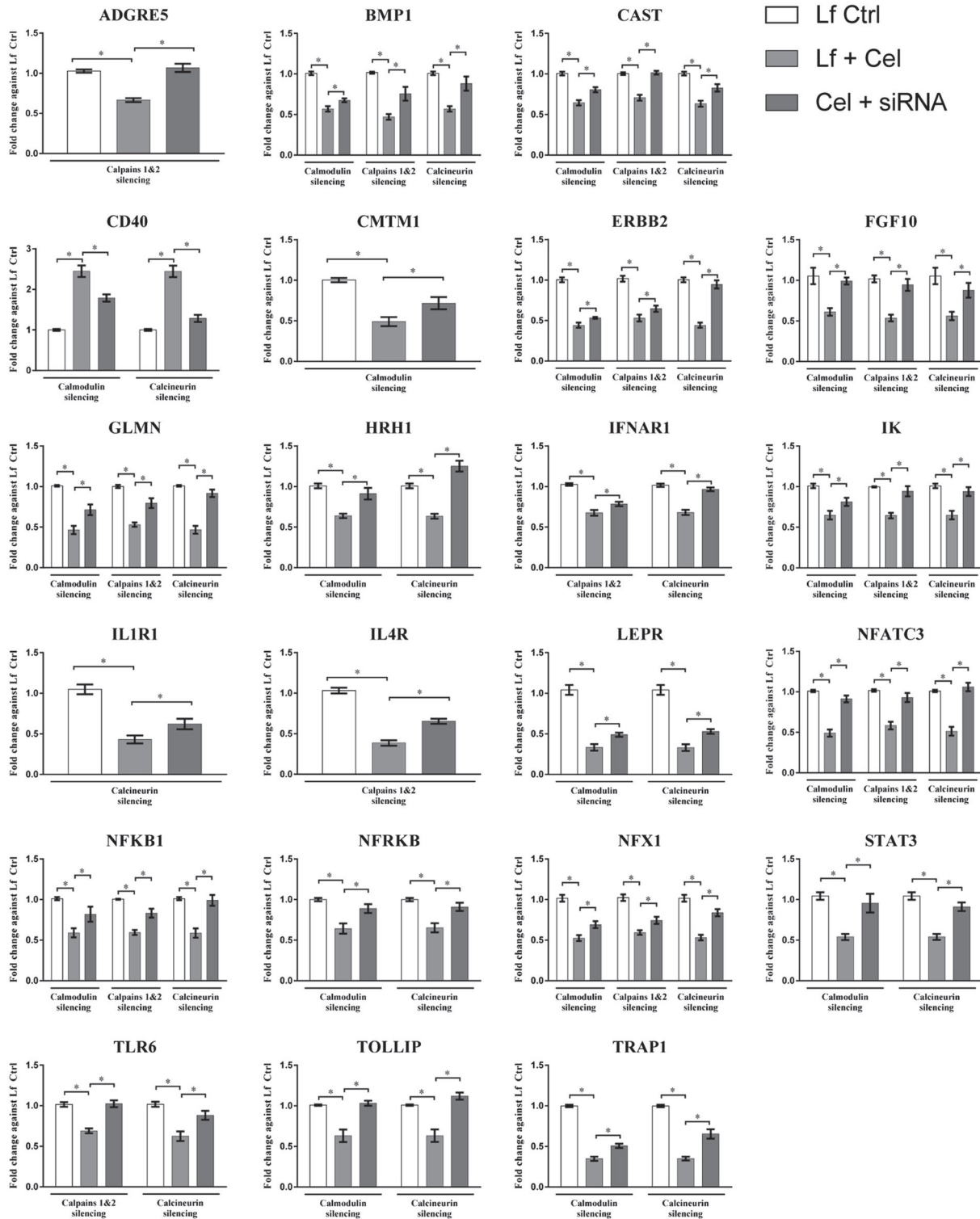


FIGURE 8 Effect of the Ca^{2+} -dependent modulators in celastrol-mediated inflammatory and autoimmunity gene expression. RAFLS were treated with celastrol (Cel; $1 \mu\text{M}$) with or without transfection of a mixture of siRNA for calmodulin genes (CALM1 + CALM2 + CALM3), calpain isoforms catalytic subunit genes (CAPN1 + CAPN2), or calcineurin isoforms catalytic subunit genes (PPP3CA + PPP3CB + PPP3CC) and compared to cells transfected with control siRNA. After RT-qPCR analysis of 22 genes associated with inflammation and autoimmunity, gene expressions were normalized to GAPDH, relative to control siRNA, and analysed using the $2^{-\Delta\Delta\text{CT}}$ method. The data are the mean \pm SEM from five independent experiments. * $P < .05$, significantly different from untreated or Cel + siRNA group

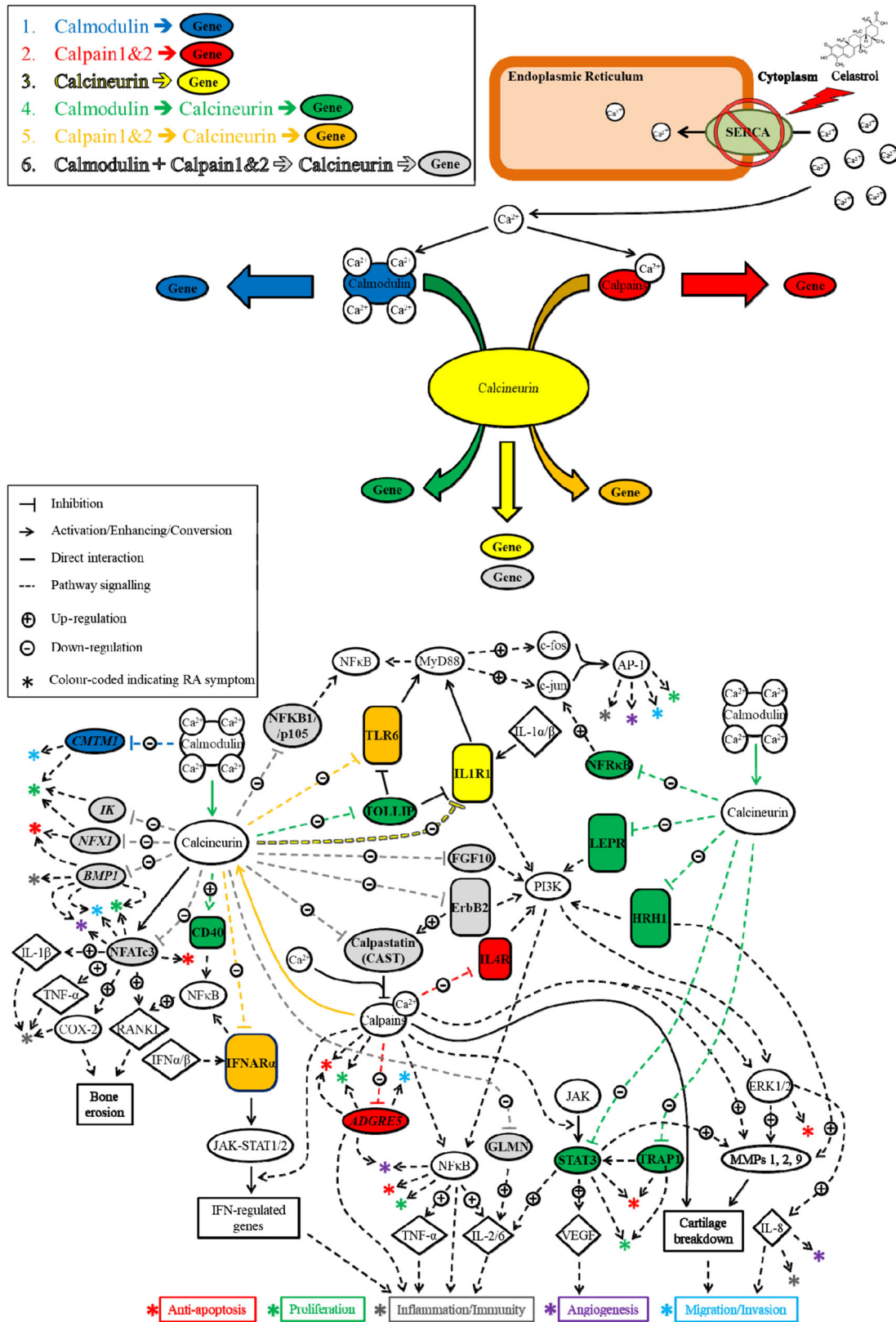


FIGURE 9 Schematic diagram showing the proposed signalling pathways for inflammatory and autoimmunity-associated gene expression via Ca²⁺ and Ca²⁺-dependent/-binding proteins. Upper part, colour-coded representation of the pathways by which the genes of interest can be affected by the calcium signalling pathway proteins in response to the cytosolic Ca²⁺ rise induced by celastrol treatment; lower part, network map linking the calcium signalling pathway proteins to their effects on the calcium-modulated genes and five RA pathogenic factors (anti-apoptosis, proliferation, inflammation and immunity, angiogenesis, migration, and invasion). Genes and pathways are colour-coded according to the upper part. RA pathogenesis factor colours are only linked to their coloured asterisks (*) and are independent of the gene and pathway colour-coding

& Moudgil, 2011; Li et al., 2012; Nanjundaiah et al., 2012; Li et al., 2013; Astry et al., 2015; Jiang et al., 2015; Lv et al., 2015). Although the molecular targets responsible for the celestrol-mediated anti-arthritis effect have been identified (Cascao et al., 2012; Li et al., 2012; Li et al., 2013; Astry et al., 2015; Cascao, Fonseca, & Moita, 2017), the mechanistic role of Ca^{2+} signalling underpinning such therapeutic effects remains unclear. Emerging evidence suggests that Ca^{2+} flux may be involved in the pathogenesis of RA. For example, significant differences in ER Ca^{2+} concentrations were found in synovial fluid T cells from patients with chronic inflammatory arthritis after T cell receptor stimulation, when compared to normal T cells (Carruthers, Arrol, Bacon, & Young, 2000). The activation of neutrophils isolated from RA patients was correlated to the Ca^{2+} entry regulated by CD147-induced modifications of lipid rafts, which modulates the downstream activation of the cation channel **TRPM7** (Wang et al., 2014). Apart from cellular activation, Ca^{2+} flux is associated with synovial accumulation of autoantigen in RA patients by triggering the activation of peptidylarginine deiminase and subsequent citrullination of vimentin in macrophages (Vossenaar et al., 2004). In addition, conformational changes resulting in altered ATPase activity of SERCA1 have been reported in AIA rats which are correlated with the systemic inflammatory status of the animal model (Strosová et al., 2011). Such observations reinforce the idea of targeting Ca^{2+} mobilization in cytoplasm or the balance of Ca^{2+} homeostasis as an alternative therapeutic approach for improving RA.

Reports from several studies have demonstrated the possibility of manipulating the activity of Ca^{2+} channels with biological agents or medicinal compounds for the treatment of RA. Wang et al. have shown that **verapamil**, a Ca^{2+} channel inhibitor, antagonized TNF- α -mediated inflammation in collagen-induced arthritis mice via the reduction of Ca^{2+} (Wang et al., 2016). The blockade of store-operated Ca^{2+} release-activated channels with the use of neutralizing antibodies can also effectively suppress the activity of T cells and B cells derived from RA patients (Liu et al., 2017). Intriguingly, ionomycin-mediated Ca^{2+} modulation enhanced the tensile properties of developing engineered articular cartilage (Natoli et al., 2010).

In this study, we examined the potential of inhibiting RA progression by manipulating Ca^{2+} homeostasis of RASFs instead of other myeloid cells, as this cell type has been shown to be extensively involved in RA pathogenesis ranging from pro-inflammatory mediator synthesis to mechanical damage of joint tissues. AIA rats were treated with celestrol given intraperitoneally, because earlier pharmacokinetic analysis demonstrated low plasma levels of celestrol after oral administration. The maximal plasma concentration (C_{max}) in a rat model with oral celestrol ($1,000 \mu\text{g}\cdot\text{kg}^{-1}$) only reached $13.75 \pm 7.94 \mu\text{g}\cdot\text{L}^{-1}$, compared with $38.83 \pm 12.83 \mu\text{g}\cdot\text{L}^{-1}$ after intravenous injection ($100 \mu\text{g}\cdot\text{kg}^{-1}$; Zhang et al., 2012). Interestingly, the absorption of celestrol was enhanced by co-treatment with other bioactive components of *Tripterygium wilfordii* Hook F (Zhang et al., 2012), providing insight to the improvement of drug delivery of celestrol. We have demonstrated that the pharmacological mechanism of celestrol in the arthritic condition involves the activation of Ca^{2+} signalling through inhibition of SERCA. Addition of the calcium chelator BAPTA/AM,

which is a highly selective agent for Ca^{2+} , leads to a partial inhibition of the therapeutic effect of celestrol in our experimental model of AIA rats. Furthermore, celestrol induced ER stress, thereby inducing apoptotic and autophagic cell death in apoptosis-resistant fibroblasts, RASFs and RAFLS, a finding that may offer an alternative way to eliminate apoptosis-resistant SLFs of RA patients. In fact, celestrol-induced cytotoxicity via the up-regulation of ER stress and **glycogen synthase kinase-3 β** signalling pathways (Feng et al., 2013), which is closely related to the phosphorylation status of the enzyme and may, in part, be regulated by **heat shock protein 90** (Zhang et al., 2008). In addition, celestrol can also target the proteasome to activate the pro-apoptotic unfolded protein response pathway and autophagy in cancer cells (Fribley et al., 2015; Wang et al., 2012). Therefore, the multi-target nature of celestrol has aroused safety concerns. In fact, the actions of celestrol appeared to be more selectively expressed in the inflammatory RAFLS and cancer cells. It is possible that the ER stress of these cells is already at a high level, such that further stimulation after celestrol exposure, may exceed a critical level leading to induction of ER stress-associated cytotoxicity. On the contrary, in normal cells exhibiting basal (low) levels of ER stress, the administration of celestrol may only up-regulate the ER stress to the cytoprotective threshold of the pathway (rather than cytotoxic levels), which could partly explain the higher tolerance towards celestrol treatment.

Downstream signalling pathways induced by the elevation of cytosolic Ca^{2+} levels are mediated by secondary Ca^{2+} sensors and calmodulin is a universal Ca^{2+} -binding protein which regulates the activity of a variety of enzymes, such as protein kinases and phosphatases, as well as other signalling proteins, including membrane receptors, channels, and structural proteins (Villalobo A, 2018). In chronic inflammatory arthritis, abnormal activation of calcineurin (a Ca^{2+} -calmodulin activated phosphatase) in synoviocytes was observed which could contribute to the corresponding pathogenesis (Yoo et al., 2006). Calpains, a set of Ca^{2+} -activated proteases, have also been shown to participate in cartilage destruction in collagen-induced arthritic knee joints of mice (Szomor, Shimizu, Fujimori, Yamamoto, & Yamamuro, 1995). Therefore, we propose that celestrol-mediated Ca^{2+} mobilization modulates a panel of inflammatory- and autoimmunity-associated genes through the Ca^{2+} -dependent/-binding proteins. Knockdown of calmodulin, calpains, and calcineurin revealed novel preliminary Ca^{2+} signalling pathways that link pharmacological targets of celestrol to their downstream gene expression based on the proposed Ca^{2+} -modulated gene network (Dias et al., 2018). The current findings not only explain the role of the reported genes but also provide a new mechanistic insight into the regulation of inflammation- and autoimmunity-associated gene expression via Ca^{2+} signalling pathways. Therefore, the ameliorating effect of celestrol in the AIA model of RA is partly attributable to Ca^{2+} -mediated autophagic cell death in apoptosis-resistant RAFLS. Celestrol may alleviate the symptoms of RA patients by down-regulation of the inflammatory response genes in RASFs via activation of Ca^{2+} signalling pathways. Notably, celestrol exhibits its therapeutic effect via targeting other immune-component cells such as regulatory T cells and Th17 cells (Astry et al., 2015; Cascao et al., 2012; Han et al., 2015) and/or other molecular pathways such as IL-

17A and NF- κ B signalling (Li et al., 2012; Li et al., 2013) as mentioned previously independent of Ca²⁺ signalling, which is supported by the observation that BAPTA/AM alone was unable to completely block the therapeutic effect of celastrol.

SERCA is a novel therapeutic target for cancer treatment, especially in multidrug-resistant tumours (Wong et al., 2013; Xu, Shao, & Zeng, 2013). The current study indicates the potential therapeutic role of SERCA in refractory RA through eliminating apoptosis- and multidrug-resistant SLFs via calcium-induced autophagic cell death. With the essential role of SERCA in maintaining normal cellular homeostasis, specific SERCA inhibitors such as thapsigargin are likely to result in significant toxicity to normal SLFs. This limitation has led to an increasing interest in the development of prodrug strategies to reduce the off-target-organ side effects and systemic toxicities (Yuan, Quan, et al., 2012). For instance, methacrylamide copolymer-based dexamethasone prodrug, hydrogen peroxide-sensitive prodrugs of MTX, and aminopterin have been synthesized for the treatment of RA. While maintaining a comparable therapeutic efficacy, these prodrugs have resulted in a safer toxicity profile and an increased the therapeutic window, compared to their parent drugs (Peiro Cadahia et al., 2018; Yuan, Nelson, et al., 2012). Therefore, it is worthwhile to further investigate whether the toxicity of celastrol can be minimized using similar prodrug strategies (Wang, Liu, Wang, He, & Chen, 2011) to provide a safer agent for treating RA patients who are less responsive to current anti-arthritis agents.

5 | CONCLUSION

This study has provided new insights into how celastrol regulates a panel of inflammatory and autoimmunity-associated genes via activation of Ca²⁺-binding/-dependent proteins. Through interlinking the possible genes regulating apoptosis, proliferation, inflammation, immunity, angiogenesis, and migration/invasion process of AIA models after treatment with celastrol, the current investigation has revealed the detailed molecular mechanisms of celastrol in the effective treatment of RA via calcium signalling.

ACKNOWLEDGEMENTS

This work was supported by a FDCT grant from the Macao Science and Technology Development Fund (Project code: 084/2013/A3).

CONFLICT OF INTEREST

The authors declare no conflicts of interest.

AUTHOR CONTRIBUTIONS

V.K.W.W., C.L.Q., and S.W.X. designed and conducted the autophagy, animal experiments, data analysis, and also drafted the manuscript. B.Y.K.L., W.Z., and H.W. carried out the AIA model experiment. F.M. conducted the SERCA activity assay and proof-reading for the whole manuscript. I.R.D.S.R.D. and S.W.F.M. performed the PCR array and real-time PCR experiments. H.P.

performed the microCT data analysis. S.H. and T.E. conducted the computational docking. Y.H., N.Z., and Y.Q.Q. performed all flow cytometry experiments. T.W.C., X.C., and L.Y. performed the western blot experiments. W.J.Y. conducted the luciferase report assay. W.Z. and Z.L. conducted the ATP metabolite experiments. Y.X. and R.L. isolated the RASFs from RA patients. Q.J. revised the manuscript and gave valuable suggestions. L.L. conceived the idea, supervised all research, and revised the manuscript.

DECLARATION OF TRANSPARENCY AND SCIENTIFIC RIGOUR

This Declaration acknowledges that this paper adheres to the principles for transparent reporting and scientific rigour of preclinical research as stated in the *BJP* guidelines for [Design & Analysis, Immunoblotting and Immunochemistry](#), and [Animal Experimentation](#), and as recommended by funding agencies, publishers and other organisations engaged with supporting research.

ORCID

Vincent Kam Wai Wong  <https://orcid.org/0000-0002-2951-8108>

REFERENCES

- Alexander, S. P. H., Christopoulos, A., Davenport, A. P., Kelly, E., Marrion, N. V., Peters, J. A., ... CGTP Collaborators. (2017). The Concise Guide to PHARMACOLOGY 2017/18: G protein-coupled receptors. *British Journal of Pharmacology*, 174, S17–S129. <https://doi.org/10.1111/bph.13878>
- Alexander, S. P. H., Fabbro, D., Kelly, E., Marrion, N. V., Peters, J. A., Faccenda, E., ... CGTP Collaborators. (2017a). The Concise Guide to PHARMACOLOGY 2017/18: Catalytic receptors. *British Journal of Pharmacology*, 174, S225–S271. <https://doi.org/10.1111/bph.13876>
- Alexander, S. P. H., Fabbro, D., Kelly, E., Marrion, N. V., Peters, J. A., Faccenda, E., ... CGTP Collaborators. (2017b). The Concise Guide to PHARMACOLOGY 2017/18: Enzymes. *British Journal of Pharmacology*, 174, S272–S359. <https://doi.org/10.1111/bph.13877>
- Alexander, S. P. H., Kelly, E., Marrion, N. V., Peters, J. A., Faccenda, E., Harding, S. D., ... CGTP Collaborators. (2017). The Concise Guide to PHARMACOLOGY 2017/18: Other proteins. *British Journal of Pharmacology*, 174, S1–S16. <https://doi.org/10.1111/bph.13882>
- Alexander, S. P. H., Striessnig, J., Kelly, E., Marrion, N. V., Peters, J. A., Faccenda, E., ... CGTP Collaborators. (2017). The Concise Guide to PHARMACOLOGY 2017/18: Voltage-gated ion channels. *British Journal of Pharmacology*, 174, S160–S194. <https://doi.org/10.1111/bph.13884>
- Arnett, F. C., Edworthy, S. M., Bloch, D. A., Mcshane, D. J., Fries, J. F., Cooper, N. S., ... Hunder, G. G. (1988). The American-Rheumatism-Association 1987 revised criteria for the classification of rheumatoid arthritis. *Arthritis and Rheumatism*, 31(3), 315–324. <https://doi.org/10.1002/art.1780310302>
- Astry, B., Venkatesha, S. H., Laurence, A., Christensen-Quick, A., Garzino-Demo, A., Frieman, M. B., ... Moudgil, K. D. (2015). Celastrol, a Chinese herbal compound, controls autoimmune inflammation by altering the balance of pathogenic and regulatory T cells in the target organ. *Clinical Immunology*, 157(2), 228–238. <https://doi.org/10.1016/j.clim.2015.01.011>
- Bartok, B., & Firestein, G. S. (2010). Fibroblast-like synoviocytes: Key effector cells in rheumatoid arthritis. *Immunological Reviews*, 233(1), 233–255. <https://doi.org/10.1111/j.0105-2896.2009.00859.x>

- Berridge, M. J. (2012). Calcium signalling remodelling and disease. *Biochemical Society Transactions*, 40, 297–309. <https://doi.org/10.1042/BST20110766>
- Carruthers, D. M., Arrol, H. P., Bacon, P. A., & Young, S. P. (2000). Dysregulated intracellular Ca²⁺ stores and Ca²⁺ signaling in synovial fluid T lymphocytes from patients with chronic inflammatory arthritis. *Arthritis and Rheumatism*, 43(6), 1257–1265. [https://doi.org/10.1002/1529-0131\(200006\)43:6<1257::AID-ANR8>3.0.CO;2-Q](https://doi.org/10.1002/1529-0131(200006)43:6<1257::AID-ANR8>3.0.CO;2-Q)
- Cascao, R., Fonseca, J. E., & Moita, L. F. (2017). Celastrol: A spectrum of treatment opportunities in chronic diseases. *Front Med (Lausanne)*, 4, 69. <https://doi.org/10.3389/fmed.2017.00069>
- Cascao, R., Vidal, B., Raquel, H., Neves-Costa, A., Figueiredo, N., Gupta, V., ... Moita, L. F. (2012). Effective treatment of rat adjuvant-induced arthritis by celastrol. *Autoimmunity Reviews*, 11(12), 856–862. <https://doi.org/10.1016/j.autrev.2012.02.022>
- Clapham, D. E. (2007). Calcium signaling. *Cell*, 131(6), 1047–1058. <https://doi.org/10.1016/j.cell.2007.11.028>
- Curtis, M. J., Alexander, S., Cirino, G., Docherty, J. R., George, C. H., Giembycz, M. A., ... Ahluwalia, A. (2018). Experimental design and analysis and their reporting II: Updated and simplified guidance for authors and peer reviewers. *British Journal of Pharmacology*, 175(7), 987–993. <https://doi.org/10.1111/bph.14153>
- Denmeade, S. R., & Isaacs, J. T. (2005). The SERCA pump as a therapeutic target: Making a “smart bomb” for prostate cancer. *Cancer Biology & Therapy*, 4(1), 14–22. <https://doi.org/10.4161/cbt.4.1.1505>
- Dias, I. R. D. R., Mok, S. W. F., Gordillo-Martinez, F., Khan, I., Hsiao, W. W. L., Law, B. Y. K., ... Liu, L. (2018). The calcium-induced regulation in the molecular and transcriptional circuitry of human inflammatory response and autoimmunity. *Frontiers in Pharmacology*, 8.
- Fang, D. D., Cao, J., Jani, J. P., Tsaparikos, K., Blasina, A., Kornmann, J., ... VanArsdale, T. (2013). Combined gemcitabine and CHK1 inhibitor treatment induces apoptosis resistance in cancer stem cell-like cells enriched with tumor spheroids from a non-small cell lung cancer cell line. *Frontiers of Medicine*, 7(4), 462–476. <https://doi.org/10.1007/s11684-013-0270-6>
- Feng, L., Zhang, D., Fan, C., Ma, C., Yang, W., Meng, Y., ... Guo, D. (2013). ER stress-mediated apoptosis induced by celastrol in cancer cells and important role of glycogen synthase kinase-3 β in the signal network. *Cell Death & Disease*, 4, e715. <https://doi.org/10.1038/cddis.2013.222>
- Fribley, A. M., Miller, J. R., Brownell, A. L., Garshott, D. M., Zeng, Q. H., Reist, T. E., ... Kaufman, R. J. (2015). Celastrol induces unfolded protein response-dependent cell death in head and neck cancer. *Experimental Cell Research*, 330(2), 412–422. <https://doi.org/10.1016/j.yexcr.2014.08.014>
- Goldbach-Mansky, R., Wilson, M., Fleischmann, R., Olsen, N., Silverfield, J., Kempf, P., ... Lipsky, P. E. (2009). Comparison of Tripterygium wilfordii Hook F versus sulfasalazine in the treatment of rheumatoid arthritis: A randomized trial. *Annals of Internal Medicine*, 151(4), 229–240. W49-51
- Han, L., Yang, J., Wang, X. W., Li, D., Lv, L., & Li, B. (2015). Th17 Cells in autoimmune diseases. *Frontiers of Medicine*, 9(1), 10–19. <https://doi.org/10.1007/s11684-015-0388-9>
- Harding, S. D., Sharman, J. L., Faccenda, E., Southan, C., Pawson, A. J., Ireland, S., ... NC-IUPHAR (2018). The IUPHAR/BPS guide to PHARMACOLOGY in 2018: Updates and expansion to encompass the new guide to IMMUNOPHARMACOLOGY. *Nucleic Acids Research*, 46(D1), D1091–D1106. <https://doi.org/10.1093/nar/gkx1121>
- Igarashi, H., Hirano, H., Yahagi, A., Saika, T., & Ishihara, K. (2014). Anti-apoptotic roles for the mutant p53R248Q through suppression of p53-regulated apoptosis-inducing protein 1 in the RA-derived fibroblast-like synoviocyte cell line MH7A. *Clinical Immunology*, 150(1), 12–21. <https://doi.org/10.1016/j.clim.2013.10.013>
- Janssen, K., Horn, S., Niemann, M. T., Daniel, P. T., Schulze-Osthoff, K., & Fischer, U. (2009). Inhibition of the ER Ca²⁺ pump forces multidrug-resistant cells deficient in Bak and Bax into necrosis. *Journal of Cell Science*, 122(Pt 24), 4481–4491. <https://doi.org/10.1242/jcs.055772>
- Jiang, M., Zha, Q., Zhang, C., Lu, C., Yan, X., Zhu, W., ... Lu, A. (2015). Predicting and verifying outcome of Tripterygium wilfordii Hook F based therapy in rheumatoid arthritis: From open to double-blinded randomized trial. *Scientific Reports*, 5, 9700. <https://doi.org/10.1038/srep09700>
- Kato, M., Ospelt, C., Gay, R. E., Gay, S., & Klein, K. (2014). Dual role of autophagy in stress-induced cell death in rheumatoid arthritis synovial fibroblasts. *Arthritis & Rheumatology*, 66(1), 40–48. <https://doi.org/10.1002/art.38190>
- Kilkenny, C., Browne, W., Cuthill, I. C., Emerson, M., Altman, D. G., & Group NCRGW (2010). Animal research: Reporting in vivo experiments: The ARRIVE guidelines. *British Journal of Pharmacology*, 160(7), 1577–1579. <https://doi.org/10.1111/j.1476-5381.2010.00872.x>
- Kim, S. K., Park, K. Y., Yoon, W. C., Park, S. H., Park, K. K., Yoo, D. H., & Choe, J. Y. (2011). Melittin enhances apoptosis through suppression of IL-6/sIL-6R complex-induced NF- κ B and STAT3 activation and Bcl-2 expression for human fibroblast-like synoviocytes in rheumatoid arthritis. *Joint, Bone, Spine*, 78(5), 471–477. <https://doi.org/10.1016/j.jbspin.2011.01.004>
- Klionsky, D. J., Abdelmohsen, K., Abe, A., Abedin, M. J., Abeliovich, H., Acevedo Arozena, A., ... Zughair, S. M. (2016). Guidelines for the use and interpretation of assays for monitoring autophagy (3rd edition). *Autophagy*, 12(1), 1–222. <https://doi.org/10.1080/15548627.2015.1100356>
- Li, G., Liu, D., Zhang, Y., Qian, Y., Zhang, H., Guo, S., ... Liu, Y. (2013). Celastrol inhibits lipopolysaccharide-stimulated rheumatoid fibroblast-like synoviocyte invasion through suppression of TLR4/NF-kappaB-mediated matrix metalloproteinase-9 expression. *PLoS ONE*, 8(7), e68905. <https://doi.org/10.1371/journal.pone.0068905>
- Li, G. Q., Zhang, Y., Liu, D., Qian, Y. Y., Zhang, H., Guo, S. Y., ... Liu, Y. Q. (2012). Celastrol inhibits interleukin-17A-stimulated rheumatoid fibroblast-like synoviocyte migration and invasion through suppression of NF- κ B-mediated matrix metalloproteinase-9 expression. *International Immunopharmacology*, 14(4), 422–431. <https://doi.org/10.1016/j.intimp.2012.08.016>
- Liu, S., Hasegawa, H., Takemasa, E., Suzuki, Y., Oka, K., Kiyoi, T., ... Maeyama, K. (2017). Efficiency and safety of CRAC inhibitors in human rheumatoid arthritis xenograft models. *Journal of Immunology*, 199(5), 1584–1595. <https://doi.org/10.4049/jimmunol.1700192>
- Lv, Q. W., Zhang, W., Shi, Q., Zheng, W. J., Li, X., Chen, H., ... Zhang, X. (2015). Comparison of Tripterygium wilfordii Hook F with methotrexate in the treatment of active rheumatoid arthritis (TRIFRA): A randomised, controlled clinical trial. *Annals of the Rheumatic Diseases*, 74(6), 1078–1086. <https://doi.org/10.1136/annrheumdis-2013-204807>
- Ma, Y., Zhou, K. H., Fan, J., & Sun, S. C. (2016). Traditional Chinese medicine: Potential approaches from modern dynamical complexity theories. *Frontiers of Medicine*, 10(1), 28–32. <https://doi.org/10.1007/s11684-016-0434-2>
- Maillefert, J. F., Maynadie, M., Tebib, J. G., Aho, S., Walker, P., Chatard, C., ... Tavernier, C. (1996). Expression of the multidrug resistance glycoprotein 170 in the peripheral blood lymphocytes of rheumatoid arthritis patients. The percentage of lymphocytes expressing glycoprotein 170 is increased in patients treated with prednisolone. *British Journal of Rheumatology*, 35(5), 430–435. <https://doi.org/10.1093/rheumatology/35.5.430>
- McGrath, J. C., & Lilley, E. (2015). Implementing guidelines on reporting research using animals (ARRIVE etc.): New requirements for

- publication in *BJP. British Journal of Pharmacology*, 172(13), 3189–3193. <https://doi.org/10.1111/bph.12955>
- Michelangeli, F., Colyer, J., East, J. M., & Lee, A. (1990). Effect of pH on the activity of the Ca²⁺ Mg²⁺ (+)-activated ATPase of sarcoplasmic reticulum. *The Biochemical Journal*, 267, 423–429. <https://doi.org/10.1042/bj2670423>
- Michelangeli, F., & East, J. M. (2011). A diversity of SERCA Ca²⁺ pump inhibitors. *Biochemical Society Transactions*, 39, 789–797. <https://doi.org/10.1042/BST0390789>
- Nanjundaiah, S. M., Venkatesha, S. H., Yu, H., Tong, L., Stains, J. P., & Moudgil, K. D. (2012). Celastrol and its bioactive celastrol protect against bone damage in autoimmune arthritis by modulating osteoimmune cross-talk. *The Journal of Biological Chemistry*, 287(26), 22216–22226. <https://doi.org/10.1074/jbc.M112.356816>
- Natoli, R. M., Skaalure, S., Bijlani, S., Chen, K. X., Hu, J., & Athanasiou, K. A. (2010). Intracellular Na⁺ and Ca²⁺ modulation increases the tensile properties of developing engineered articular cartilage. *Arthritis and Rheumatism*, 62(4), 1097–1107. <https://doi.org/10.1002/art.27313>
- Peiro Cadahia, J., Bondebjerg, J., Hansen, C. A., Previtali, V., Hansen, A. E., Andresen, T. L., & Clausen, M. H. (2018). Synthesis and evaluation of hydrogen peroxide sensitive prodrugs of methotrexate and aminopterin for the treatment of rheumatoid arthritis. *Journal of Medicinal Chemistry*, 61(8), 3503–3515. <https://doi.org/10.1021/acs.jmedchem.7b01775>
- Sakaguchi, N., Takahashi, T., Hata, H., Nomura, T., Tagami, T., Yamazaki, S., ... Sakaguchi, S. (2003). Altered thymic T-cell selection due to a mutation of the ZAP-70 gene causes autoimmune arthritis in mice. *Nature*, 426(6965), 454–460. <https://doi.org/10.1038/nature02119>
- Stammers, A. N., Susser, S. E., Hamm, N. C., Hlynsky, M. W., Kimber, D. E., Kehler, D. S., & Duhamel, T. A. (2015). The regulation of sarco (endo) plasmic reticulum calcium-ATPases (SERCA). *Canadian Journal of Physiology and Pharmacology*, 93(10), 843–854. <https://doi.org/10.1139/cjpp-2014-0463>
- Strosova, M. K., Karlovska, J., Zizkova, P., Kwolek-Mirek, M., Ponist, S., Spickett, C. M., & Horakova, L. (2011). Modulation of sarcoplasmic/endoplasmic reticulum Ca(2+)-ATPase activity and oxidative modification during the development of adjuvant arthritis. *Archives of Biochemistry and Biophysics*, 511(1–2), 40–47. <https://doi.org/10.1016/j.abb.2011.04.011>
- Szomor, Z., Shimizu, K., Fujimori, Y., Yamamoto, S., & Yamamuro, T. (1995). Appearance of calpain correlates with arthritis and cartilage destruction in collagen induced arthritic knee joints of mice. *Annals of the Rheumatic Diseases*, 54(6), 477–483. <https://doi.org/10.1136/ard.54.6.477>
- Tao, X., & Lipsky, P. E. (2000). The Chinese anti-inflammatory and immunosuppressive herbal remedy *Tripterygium wilfordii* Hook F. *Rheumatic Diseases Clinics of North America*, 26(1), 29–50, viii. [https://doi.org/10.1016/S0889-857X\(05\)70118-6](https://doi.org/10.1016/S0889-857X(05)70118-6)
- Tao, X., Younger, J., Fan, F. Z., Wang, B., & Lipsky, P. E. (2002). Benefit of an extract of *Tripterygium Wilfordii* Hook F in patients with rheumatoid arthritis: A double-blind, placebo-controlled study. *Arthritis and Rheumatism*, 46(7), 1735–1743. <https://doi.org/10.1002/art.10411>
- Todd, D. J., Lee, A. H., & Glimcher, L. H. (2008). The endoplasmic reticulum stress response in immunity and autoimmunity. *Nature Reviews Immunology*, 8(9), 663–674. <https://doi.org/10.1038/nri2359>
- Tolboom, T. C. A., van der Helm-Van Mil, A. H., Nelissen, R. G. H. H., Breedveld, F. C., Toes, R. E. M., & Huizinga, T. W. J. (2005). Invasiveness of fibroblast-like synoviocytes is an individual patient characteristic associated with the rate of joint destruction in patients with rheumatoid arthritis. *Arthritis and Rheumatism*, 52(7), 1999–2002. <https://doi.org/10.1002/art.21118>
- Tsokos, G. C. (2011). Systemic lupus erythematosus. *The New England Journal of Medicine*, 365(22), 2110–2121. <https://doi.org/10.1056/NEJMra1100359>
- Tsujimura, S., Saito, K., Nawata, M., Nakayama, S., & Tanaka, Y. (2008). Overcoming drug resistance induced by P-glycoprotein on lymphocytes in patients with refractory rheumatoid arthritis. *Annals of the Rheumatic Diseases*, 67(3), 380–388. <https://doi.org/10.1136/ard.2007.070821>
- Turner, J. D., & Filer, A. (2015). The role of the synovial fibroblast in rheumatoid arthritis pathogenesis. *Current Opinion in Rheumatology*, 27(2), 175–182. <https://doi.org/10.1097/BOR.0000000000000148>
- Venkatesha, S. H., Yu, H., Rajaiah, R., Tong, L., & Moudgil, K. D. (2011). Celastrol-derived celastrol suppresses autoimmune arthritis by modulating antigen-induced cellular and humoral effector responses. *The Journal of Biological Chemistry*, 286(17), 15138–15146. <https://doi.org/10.1074/jbc.M111.226365>
- Villalobo, A., Ishida, H., Vogel, H. J., & Berchtold, M. W. (2018). Calmodulin as a protein linker and a regulator of adaptor/scaffold proteins. *Biochimica et Biophysica Acta*, (3), 1865.
- Vossenaar, E. R., Radstake, T. R. D., van der Heijden, A., van Mansum, M. A. M., Dieteren, C., de Rooij, D. J., ... van Venrooij, W. (2004). Expression and activity of citrullinating peptidylarginine deiminase enzymes in monocytes and macrophages. *Annals of the Rheumatic Diseases*, 63(4), 373–381. <https://doi.org/10.1136/ard.2003.012211>
- Wang, C. H., Rong, M. Y., Wang, L., Ren, Z., Chen, L. N., Jia, J. F., ... Zhu, P. (2014). CD147 up-regulates calcium-induced chemotaxis, adhesion ability and invasiveness of human neutrophils via a TRPM-7-mediated mechanism. *Rheumatology*, 53(12), 2288–2296. <https://doi.org/10.1093/rheumatology/keu260>
- Wang, S., Liu, K., Wang, X., He, Q., & Chen, X. (2011). Toxic effects of celastrol on embryonic development of zebrafish (*Danio rerio*). *Drug and Chemical Toxicology*, 34(1), 61–65. <https://doi.org/10.3109/01480545.2010.494664>
- Wang, W., Li, Z., Meng, Q., Zhang, P., Yan, P., Zhang, Z., ... Zhao, Y. (2016). Chronic calcium channel inhibitor verapamil antagonizes TNF- α -mediated inflammatory reaction and protects against inflammatory arthritis in mice. *Inflammation*, 39(5), 1624–1634. <https://doi.org/10.1007/s10753-016-0396-1>
- Wang, W. B., Feng, L. X., Yue, Q. X., Wu, W. Y., Guan, S. H., Jiang, B. H., ... Guo, D. A. (2012). Paraptosis accompanied by autophagy and apoptosis was induced by celastrol, a natural compound with influence on proteasome, ER stress and Hsp90. *Journal of Cellular Physiology*, 227(5), 2196–2206. <https://doi.org/10.1002/jcp.22956>
- Wong, V. K., Li, T., Law, B. Y., Ma, E. D., Yip, N. C., Michelangeli, F., ... Liu, L. (2013). Saikosaponin-d, a novel SERCA inhibitor, induces autophagic cell death in apoptosis-defective cells. *Cell Death & Disease*, 4, e720. <https://doi.org/10.1038/cddis.2013.217>
- Xu, M., Shao, J. Y., & Zeng, Y. X. (2013). Molecular classification and molecular targeted therapy of cancer. *Frontiers of Medicine*, 7(2), 147–149. <https://doi.org/10.1007/s11684-013-0274-2>
- Yoo, S. A., Park, B. H., Park, G. S., Koh, H. S., Lee, M. S., Ryu, S. H., ... Kim, W. U. (2006). Calcineurin is expressed and plays a critical role in inflammatory arthritis. *Journal of Immunology*, 177(4), 2681–2690. <https://doi.org/10.4049/jimmunol.177.4.2681>
- Yuan, F., Nelson, R. K., Tabor, D. E., Zhang, Y., Akhter, M. P., Gould, K. A., & Wang, D. (2012). Dexamethasone prodrug treatment prevents nephritis in lupus-prone (NZB x NZW)F1 mice without causing systemic side effects. *Arthritis and Rheumatism*, 64(12), 4029–4039. <https://doi.org/10.1002/art.34667>

- Yuan, F., Quan, L. D., Cui, L., Goldring, S. R., & Wang, D. (2012). Development of macromolecular prodrug for rheumatoid arthritis. *Advanced Drug Delivery Reviews*, 64(12), 1205–1219. <https://doi.org/10.1016/j.addr.2012.03.006>
- Zhang, J., Li, C. Y., Xu, M. J., Wu, T., Chu, J. H., Liu, S. J., & Ju, W. Z. (2012). Oral bioavailability and gender-related pharmacokinetics of celastrol following administration of pure celastrol and its related tablets in rats. *Journal of Ethnopharmacology*, 144(1), 195–200. <https://doi.org/10.1016/j.jep.2012.09.005>
- Zhang, T., Hamza, A., Cao, X. H., Wang, B., Yu, S. W., Zhan, C. G., & Sun, D. (2008). A novel Hsp90 inhibitor to disrupt Hsp90/Cdc37 complex against pancreatic cancer cells. *Molecular Cancer Therapeutics*, 7(1), 162–170. <https://doi.org/10.1158/1535-7163.MCT-07-0484>

SUPPORTING INFORMATION

Additional supporting information may be found online in the Supporting Information section at the end of the article.

How to cite this article: Wong VKW, Qiu C, Xu S-W, et al. Ca^{2+} signalling plays a role in celastrol-mediated suppression of synovial fibroblasts of rheumatoid arthritis patients and experimental arthritis in rats. *Br J Pharmacol*. 2019;176: 2922–2944. <https://doi.org/10.1111/bph.14718>